

Quasielastic axial-vector mass from experiments on neutrino–nucleus scattering.

K. S. Kuzmin^{1,2,a}, V. V. Lyubushkin^{3,4,b}, and V. A. Naumov^{1,c}

¹ Bogoliubov Laboratory of Theoretical Physics, Joint Institute for Nuclear Research, RU-141980 Dubna, Russia

² Institute for Theoretical and Experimental Physics, RU-117259 Moscow, Russia

³ Dzhelepov Laboratory of Nuclear Problems, Joint Institute for Nuclear Research, RU-141980 Dubna, Russia

⁴ Physics Department of Irkutsk State University, RU-664003, Irkutsk, Russia

Received: December 29, 2007

Abstract. We analyse available experimental data on the total and differential charged-current cross sections for quasielastic $\nu_\mu N$ and $\bar{\nu}_\mu N$ scattering, obtained with a variety of nuclear targets in the accelerator experiments at ANL, BNL, FNAL, CERN, and IHEP, dating from the end of sixties to the present day. The data are used to adjust the poorly known value of the axial-vector mass of the nucleon.

1 Introduction

A precise knowledge of the cross sections for charged-current induced quasielastic scattering (QES) of neutrinos and antineutrinos on nuclear targets is a pressing demand of the current and planning next generation experiments with accelerator and atmospheric neutrino beams, aiming at the further exploration of neutrino oscillations, probing nonstandard neutrino interactions, searches for proton decay, and related phenomena.

The quasielastic cross sections are very sensitive to the poorly known shape of the weak axial-vector form factor $F_A(Q^2)$ of the nucleon. Adopting the conventional dipole approximation, this form factor is determined by the axial-vector coupling $g_A = F_A(0)$ and the phenomenological parameter M_A , the so-called axial-vector (dipole) mass related to the root-mean-square axial radius by

$$\langle r_A^2 \rangle = -\frac{6}{g_A} \left[\frac{dF_A(Q^2)}{dQ^2} \right]_{Q^2=0} = \frac{12}{M_A^2}.$$

The experimental values of M_A extracted from neutrino and antineutrino scattering data and from the more involved and vastly model-dependent analyses of charged pion electroproduction off protons, show very wide spread, from roughly 0.7 to 1.2 GeV with the formal weighted averages [1, 2]

$$M_A = \begin{cases} 1.026 \pm 0.021 \text{ GeV} & \text{from } \nu_\mu, \bar{\nu}_\mu \text{ experiments,} \\ 1.069 \pm 0.016 \text{ GeV} & \text{from } \pi \text{ electroproduction.} \end{cases}$$

The first value, the common default in most current neutrino simulations, is defined largely by $\nu_\mu d$ bubble cham-

ber experiments; in many of these experiments, the extractions of M_A were based on the naive dipole approximation for the vector form factors of the nucleon, along with other conjectures. The second value should be in fact decreased by about 5%, in order to account for hadronic loop corrections (see, e.g., Ref. [1]).

The results of several selected $\nu_\mu d$, $\bar{\nu}_\mu H$, and π^\pm electroproduction experiments have been recently reanalyzed by Bodek et al. [3], using a new improved description of the vector form factors (“BBBA(07)” parametrization). The obtained world average axial mass is

$$M_A = 1.014 \pm 0.014 \text{ GeV} \quad (\text{BBBA(07)}).$$

This value seems to be in conflict with the new results of high-statistics neutrino experiments K2K SciFi [4] (oxygen target) and MiniBooNE [5] (carbon target), reported unexpectedly large while mutually consistent values of the axial mass:

$$M_A = \begin{cases} 1.20 \pm 0.12 \text{ GeV} & (\text{K2K}), \\ 1.23 \pm 0.20 \text{ GeV} & (\text{MiniBooNE}) \end{cases}$$

A preliminary analysis of antineutrino data in MiniBooNE yields a consistent value of M_A [6].

Both K2K and MiniBooNE extractions utilize the *updated* vector form factors, from Refs. [7, 8] and [9], respectively. Within the low- Q^2 regions explored in K2K and MiniBooNE experiments, the difference between these parametrizations and BBBA(07) is comparatively small.

It can be noted that nuclear effects in the K2K analysis were accounted within the standard relativistic Fermi gas (RFG) model [10], while the MiniBooNE analysis used RFG modified by including an “instrumental” free parameter κ which changes the strength of Pauli-blocking. A fit of the Q^2 shape above 0.25 GeV² (where the variations of

^a e-mail: KKuzmin@jinr.theor.ru

^b e-mail: Vladimir.Lyubushkin@cern.ch

^c e-mail: VNaumov@jinr.theor.ru

κ has no significant impact) leads to an even larger value of $M_A = 1.25 \pm 0.12$ GeV.

In this study, which is in a sense complementary to that by Bodek et al. [3], we attempt to extract the axial mass value by a global statistical analysis of all available consistent data on the total and differential QES cross sections measured in accelerator experiments with ν_μ and $\bar{\nu}_\mu$ beams¹ from ANL [11, 12, 13, 14, 15, 16, 17, 18], BNL [19, 20, 21, 22, 23, 24, 25, 26, 27, 28, 29, 30], FNAL [31, 32, 33, 34, 35, 36, 37], CERN [38, 39, 40, 41, 42, 43, 44, 45, 46, 47, 48, 49, 50, 51, 52, 53, 54, 55, 56, 57, 58, 59, 60, 61], and IHEP [62, 63, 64, 65, 66, 67, 68, 69, 70, 71]. The detector media used in these experiments are hydrogen, deuterium, carbon, aluminium, argon, iron/steel, propane, freon, and also propane–freon and neon–hydrogen mixtures.

In the likelihood analysis, we use the most accurate phenomenological parametrizations for the vector form factors of the nucleon [72, 73], we take into account all known sources of uncertainties, in particular, the systematic errors in the energy spectra of ν_μ and $\bar{\nu}_\mu$ beams. For description of nuclear effects we apply the standard RFG model. We examine possible difference between the values of M_A extracted from ν_μ and $\bar{\nu}_\mu$ data, and cross-check our results with the data on Q^2 distributions measured in several experiments.

2 Quasielastic neutrino scattering off free nucleon

2.1 Structure functions and cross section

Let us first summarize the well-known phenomenology for describing the hypercharge conserved quasielastic reactions on free nucleon targets

$$\begin{aligned} \nu_\ell(k) + n(p) &\rightarrow \ell^-(k') + p(p'), \\ \bar{\nu}_\ell(k) + p(p) &\rightarrow \ell^+(k') + n(p'). \end{aligned} \quad (1)$$

Here k, k', p , and p' denote the four-momenta and ℓ stays for e, μ , or τ . In this paper, we will neglect the proton-neutron mass difference,² since the resulting correction, in the $\nu_\mu/\bar{\nu}_\mu$ case, exclusively works near the reaction threshold and practically negligible for the energies of our current interest. The general formulas which take this effect into account, were derived in Ref. [74] (assuming T and C invariance) and in Refs. [75, 76] (avoiding these assumptions).

The double differential cross-section for these processes is a convolution of spin-averaged leptonic and hadronic tensors $L_{\alpha\beta}$ and $W_{\alpha\beta}$:

$$\frac{d\sigma_{\text{free}}}{dE_\ell d\cos\theta_\ell} = \frac{G_F^2 P_\ell}{\pi(1 + Q^2/M_W^2)^2} \left(\frac{L^{\alpha\beta} W_{\alpha\beta}}{4ME_\nu} \right). \quad (2)$$

¹ The $\nu_e, \bar{\nu}_e, \nu_\tau$, and $\bar{\nu}_\tau$ beams from past and current accelerator experiments are not appropriate for measuring the QES cross sections.

² While our computer code operates with the most general formulas and relevant kinematics.

Here G_F is the Fermi coupling, $q = k - k'$ is the four-momentum transferred from the incoming (anti)neutrino to the nucleon, $Q^2 = -q^2$, M_W is the mass of intermediate W -boson; $E_\nu, E_\ell, P_\ell = \sqrt{E_\ell^2 - m_\ell^2}$, and θ_ℓ are, respectively, the incident (anti)neutrino energy, outgoing lepton energy, momentum, and scattering angle in the lab frame, m_ℓ is the lepton mass. The leptonic tensor defined by the product of the weak leptonic currents, is given by

$$L_{\alpha\beta}(k, k') = 2 [k'_\alpha k_\beta + k_\alpha k'_\beta - g_{\alpha\beta}(kk') \mp i\varepsilon_{\alpha\beta\gamma\delta} k^\gamma k'^\delta], \quad (3)$$

where the upper (lower) sign is for ν_ℓ ($\bar{\nu}_\ell$). Assuming the isotopic invariance, the hadronic tensor is defined by the six structure functions $W_i(Q^2)$:

$$\begin{aligned} W_{\alpha\beta}(p, q) = & -g_{\alpha\beta}W_1 + \frac{p_\alpha p_\beta}{M^2}W_2 \\ & - \frac{i\varepsilon_{\alpha\beta\gamma\delta} p^\gamma q^\delta}{2M^2}W_3 + \frac{q_\alpha q_\beta}{M^2}W_4 \\ & + \frac{p_\alpha q_\beta + q_\alpha p_\beta}{2M^2}W_5 + i \frac{p_\alpha q_\beta - q_\alpha p_\beta}{2M^2}W_6, \end{aligned} \quad (4)$$

where M is the mass of the “isoscalar” nucleon. Then combining Eqs. (3) and (4) yields

$$\begin{aligned} \frac{L^{\alpha\beta} W_{\alpha\beta}}{4ME_\nu} = & \left(\frac{E_\ell - P_\ell \cos\theta_\ell}{M} \right) (W_1 + 2\kappa^2 W_4) \\ & \pm \left[\left(\frac{E_\nu + E_\ell}{M} \right) \left(\frac{E_\ell - P_\ell \cos\theta_\ell}{2M} \right) - 2\kappa^2 \right] W_3 \\ & + \frac{E_\ell + P_\ell \cos\theta_\ell}{2M} W_2 - 2\kappa^2 W_5, \end{aligned} \quad (5)$$

where $\kappa = m_\ell/2M$.

In order to connect the structure functions with the nucleon form factors, we define the charged hadronic current for the QES process (see, e.g., Ref. [77]):

$$\langle p(p') | J_\alpha | n(p) \rangle = V_{ud} \bar{u}_p(p') \Gamma_\alpha(p, q) u_n(p). \quad (6)$$

Here V_{ud} is the ud transition element from the Cabibbo-Kobayashi-Maskawa quark-mixing matrix and

$$\begin{aligned} \Gamma_\alpha(p, q) = & \gamma_\alpha F_V + i\sigma_{\alpha\beta} \frac{q^\beta}{2M} F_M + \frac{q_\alpha}{M} F_S \\ & + \left(\gamma_\alpha F_A + \frac{p_\alpha + p'_\alpha}{M} F_T + \frac{q_\alpha}{M} F_P \right) \gamma_5. \end{aligned} \quad (7)$$

The form factors F_i are in general complex functions of Q^2 . After standard calculations one finds

$$W_i(Q^2) = 2M^2 |V_{ud}|^2 w_i(Q^2) \delta(2(pq) - Q^2), \quad (8)$$

with

$$\begin{aligned}
w_1 &= |F_A|^2 + x' (|F_V + F_M|^2 + |F_A|^2), \\
w_2 &= |F_V|^2 + |F_A|^2 + x' (|F_M|^2 + 4|F_T|^2), \\
w_3 &= -2\text{Re}[F_A^*(F_V + F_M)], \\
w_4 &= \frac{1}{4} [x' (|F_M - 2F_S| + 4|F_P + F_T|^2) - |F_M|^2] \\
&\quad + |F_S|^2 + \frac{1}{2}\text{Re}[F_V^*(2F_S - F_M) - 2F_A^*(F_P + F_T)], \\
w_5 &= w_2 + 2\text{Re}[F_S^*(F_V - x'F_M) - F_T^*(F_A - 2x'F_P)], \\
w_6 &= 2\text{Im}[F_S^*(F_V - x'F_M) + F_T^*(F_A - 2x'F_P)],
\end{aligned}$$

and $x' = Q^2/4M^2$. The only difference between this result and that from Ref. [77] is in the relative sign of the terms in ω_6 which does not contribute to the QES cross section.³

Inserting Eqs. (5) and (8) into Eq. (2) gives the commonly known formula for the differential cross section for reactions (1) on free nucleon targets:

$$\begin{aligned}
\frac{d\sigma_{\text{free}}}{dQ^2} &= \frac{G_F^2 M^2 |V_{ud}|^2}{8\pi(1 + Q^2/M_W^2)^2 E_\nu} \\
&\quad \times \left[A \frac{m_\ell^2 + Q^2}{M^2} + B \frac{s - u}{M^2} + C \frac{(s - u)^2}{M^4} \right],
\end{aligned}$$

where

$$\begin{aligned}
A &= 2x'|F_V + F_M|^2 - (1 + x')|F_V|^2 - x'(1 + x')|F_M|^2 \\
&\quad + (1 + x')|F_A|^2 - 4x'(1 + x')|F_T|^2 \\
&\quad - \kappa^2 [|F_V + F_M|^2 + |F_A + 2F_P|^2 \\
&\quad - 4(1 + x')(|F_A|^2 + |F_P|^2)], \\
B &= \mp 4x'\text{Re}[F_A^*(F_V + F_M)] \\
&\quad + 4\kappa^2\text{Re}[F_T^*(F_A - x'F_P) - F_S^*(F_V - x'F_M)], \\
C &= \frac{1}{4} (|F_V|^2 + x'|F_M|^2 + |F_A|^2 + 4x'|F_T|^2), \\
s &= (k + p)^2 = 2ME_\nu + M^2, \\
u &= (k' - p)^2 = m_\ell^2 - 2ME_\ell = m_\ell^2 - 2ME_\nu + Q^2.
\end{aligned}$$

2.2 Induced scalar and tensor form factors

The quoted formulas take into account the nonstandard G parity violating axial and vector second-class currents (SCC) which induce the nonzero scalar and tensor form factors F_S and F_T . The most robust restrictions on the SCC couplings $F_{S,T}(0)$ come from the studies of β decay of complex nuclei (see, e.g., Refs. [78,79] and quoted therein references). However, these studies are almost insensitive to the SCC effects at nonzero Q^2 . The latter were investigated in several (anti)neutrino experiments at BNL [22,

25,26,27] ($Q^2 \lesssim 1.2 \text{ GeV}^2$) and in the IHEP-ITEP spark chamber experiment at Serpukhov [68] ($Q^2 \lesssim 2.4 \text{ GeV}^2$), adopting the *ad hoc* dipole parameterizations

$$\begin{aligned}
F_S(Q^2) &= \xi_S F_V(0) (1 + Q^2/M_S^2)^{-2}, \\
F_T(Q^2) &= \xi_T F_A(0) (1 + Q^2/M_T^2)^{-2}.
\end{aligned}$$

The strongest (but yet not too telling) 90% C.L. upper limit for the axial SCC strength ξ_T has been obtained at the BNL AGS $\bar{\nu}_\mu$ experiment [27] as a function of the “tensor mass” M_T , assuming conservation of vector current (CVC) (that is $\xi_S = 0$), and simple dipole form for the vector and axial form factors with $M_V = 0.84 \text{ GeV}$ and $M_A = 1.09 \text{ GeV}$. The limit ranges between 0.78 at $M_T = 0.5 \text{ GeV}$ to about 0.11 at $M_T = 1.5 \text{ GeV}$. In so much as the contribution of the scalar form factor into the QES cross section is suppressed by $(m_\mu/M)^2 \approx 0.01$, the 90% C.L. constraint to the vector SCC strength ξ_S is even less impressive: $\xi_S < 1.9$, assuming $\xi_T = 0$, $M_S = 1 \text{ GeV}$, and the same M_V and M_A as above.

Below, keeping in mind this vagueness, we will assume the time and charge invariance of the hadronic current. Under this standard assumption, all the form factors are real functions of Q^2 and

$$F_S = F_T = 0.$$

2.3 Vector form factors

The Dirac and Pauli form factors $F_{V,M}$ are related to the Sachs electric and magnetic form factors $G_{E,M}$:

$$F_V = \frac{G_E + x'G_M}{1 + x'}, \quad F_M = \frac{G_M - G_E}{1 + x'}.$$

Isotopic symmetry provides simple relation between $G_{E,M}$ and elastic electric and magnetic form factors of proton and neutron $G_E^{p,n}$ and $G_M^{p,n}$:

$$G_M = G_M^p - G_M^n, \quad G_E = G_E^p - G_E^n.$$

At low Q^2 , a reasonable description of the electric and magnetic form factors is given by the dipole approximation:

$$G_E^p \approx G_D, \quad G_M^p \approx \mu_p G_D, \quad G_E^n \approx 0, \quad G_M^n \approx \mu_n G_D,$$

where $G_D = (1 + Q^2/M_V^2)^{-2}$, $M_V = 0.84 \text{ GeV}$, and μ_p (μ_n) is the anomalous magnetic moment of the proton (neutron). Analyses of the almost all earlier neutrino experiments were based on this approximation. In this study, we utilize two more sophisticated models for the form factors $G_E^{p,n}$ and $G_M^{p,n}$ – BBBA(07) [72] and GKex(05)[73].

The BBBA(07) model is an accurate Kelly type parametrization of the current experimental data on the form factors G_E^p , G_M^p , G_E^n , G_M^n , and ratio G_E^p/G_M^p , which uses the Nachtmann scaling variable

$$\xi_{p,n} = 2 \left(1 + \sqrt{1 + 4M_{p,n}^2/Q^2} \right)^{-1}$$

³ According to Llewellyn Smith, the functions $\omega'_5 = \omega_5 - \omega_2$ and ω_6 are, respectively, the real and imaginary parts of a unique function. Our examination does not confirm this property for the general case of nonvanishing second-class current induced form factors F_S and F_T .

to relate elastic and inelastic form factors, and imposes quark-hadron duality asymptotic constraints at high momentum transfers where the quark structure dominates. The parametrization is based on the same datasets as were used by Kelly [80], updated to include some recent experimental results. Quark-hadron duality implies that the squared ratio of neutron and proton magnetic form factors should be the same as the ratio of the corresponding inelastic structure functions F_2^n and F_2^p in the limit $\xi_{p,n} = 1$:

$$\left(\frac{G_M^n}{G_M^p}\right)^2 = \frac{F_2^n}{F_2^p} = \frac{1 + 4(d/u)}{4 + (d/u)}, \quad Q^2 \rightarrow \infty.$$

Here d and u are the partonic density functions. The authors fit the data under the two assumptions: $d/u = 0$ and $d/u = 0.2$. One more duality-motivated constraint is the equality

$$(G_E^n/G_M^n)^2 = (G_E^p/G_M^p)^2$$

applied for the highest Q^2 data points for the neutron electric form factor included into the BBBA(07) fit.

The GKex(05) model is in fact a modification of the QCD inspired vector dominance model (VDM) by Gari and Krümpelmann (GK) [81] extended and fine-tuned by Lomon [82,83] in order to match the current and consistent earlier experimental data. The data set used by Lomon includes the polarization transfer measurements, which are directly related to the ratios of electric to magnetic form factors, and differential cross section measurements of the magnetic form factors. The electric form factors derived from the Rosenbluth separation of the differential cross section are only used for the lower range of Q^2 where the magnetic contributions are less dominant. Among several versions of the parametrization considered by Lomon, we chose the latest one “GKex(05)” described in Ref. [73]. This version incorporates the data that has become available since the publication [83] and has a bit better χ^2 . The fitted parameters agree with the known constraints and the model is consistent with VDM at low Q^2 , while approaching perturbative QCD behavior at high Q^2 . The quark-hadron duality constraint is not imposed.

Figure 1 shows a comparison of the GKex(05) and BBBA(07) parametrizations for the form factors $G_E^{p,n}$ and $G_M^{p,n}$ divided by the standard dipole G_D , against the experimental data extracted using either the Rosenbluth separation or polarization transfer techniques (including a series of double-polarization measurements of neutron knock-out from a polarized ^2H or ^3He targets). The data assemblage is borrowed from Refs. [84,85,86,87] and recent reviews [88,89]. It is seen from the figure that the models are numerically close to each other at low momentum transfers covered by experiment, but diverge at high Q^2 . The most serious disagreement between the models is in the neutron electric form factor at $Q^2 \gtrsim 2 \text{ GeV}^2$. In section 4, we examine how the model differences affect the extracted value of the axial mass.

2.4 Axial-vector and induced pseudoscalar form factors

For the axial and pseudoscalar form factors we use the conventional parametrizations [77]

$$F_A(Q^2) = F_A(0) \left(1 + \frac{Q^2}{M_A^2}\right)^{-2}, \quad (9)$$

$$F_P(Q^2) = \frac{2M^2}{m_\pi^2 + Q^2} F_A(Q^2), \quad (10)$$

where $F_A(0) = g_A$ is the axial coupling, m_π is the charged pion mass, and M_A is the axial-vector mass treated as a free parameter. In fact, Eq. (10) is a conjecture inspired by the hypothesis of partial conservation of the axial current (PCAC), expectation that the form factor F_P is dominated by the pion pole near $Q^2 = 0$, and the “technical” condition

$$m_\pi^2 \left| \frac{1}{F_A(0)} \frac{dF_A(Q^2)}{dQ^2} \right|_{Q^2=0} = \frac{2m_\pi^2}{M_A^2} \ll 1,$$

which is obviously fulfilled for the experimental lower limit of M_A . Since the pseudoscalar contribution enters into the cross sections multiplied by $(m_\ell/M)^2$, the uncertainty caused by this approximation may only be important for $\nu_\tau/\bar{\nu}_\tau$ induced reactions (especially in the low- Q^2 range, see, e.g., Refs. [90,91]) and it is insignificant for reactions induced by electron and muon (anti)neutrinos.

2.5 Constants

The most precise determination of V_{ud} comes from superallowed nuclear beta decays ($0^+ \rightarrow 0^+$ transitions). We adopt the weighted average of the nine best measured superallowed decays $V_{ud}^{(\text{SA})} = 0.97377 \pm 0.00027$ recommended by the Particle Data Group (PDG) [92]. Note that this value is consistent with that of the PIBETA experiment at PSI [93], $V_{ud}^{(\text{PIBETA})} = 0.9728 \pm 0.0030$, obtained from the measured branching ratio for pion beta decay $\pi^+ \rightarrow \pi^0 e^+ \nu$.

For the axial-vector and Fermi coupling constants, we use the standard PDG averaged values: $g_A = -1.2695 \pm 0.0029$ and $G_F = 1.16637 \times 10^{-5} \text{ GeV}^2$ [92]. In several papers (see, e.g., Ref. [94] and references therein) it is suggested to use the value $G'_F = 1.1803 \times 10^{-5} \text{ GeV}^2$ obtained from $0^+ \rightarrow 0^+$ nuclear β decays, rather than the standard G_F obtained from muon β decay. The coupling constant G'_F subsumes the bulk of the inner radiative corrections. However, some neutrino experiments already take the radiative corrections into account (sometimes in quite different ways) in the measured cross sections. That is why, in this study, we simply add the corresponding difference (of about 2%) to the overall uncertainty of the fit. Note that using the G'_F instead of G_F would lead to a few percent decrease of the output value of M_A .

3 Relativistic Fermi gas model

Since the main part of the experimental data on the QES cross sections for nuclear targets was not corrected for nuclear effects, we must take these into account in our calculations. In the present work, we use the RFG model by Smith and Moniz [10] incorporated as a standard tool into essentially all neutrino event generators employed in accelerator and astroparticle neutrino experiments.

According to RFG, the hadronic tensor $W_{\alpha\beta}$ given by Eq. (4) must be replaced with the tensor $T_{\alpha\beta}$, which describes the bound nucleon. This tensor is of the same Lorentz structure as $W_{\alpha\beta}$ and is defined by the six invariant nuclear structure functions $T_i(Q^2)$. Thus, in the in the lab. frame

$$\begin{aligned} T_{\alpha\beta}(p_{\text{lab}}, q) &= -g_{\alpha\beta}T_1 + g_{0\alpha}g_{0\beta}T_2 \\ &\quad - \frac{i\varepsilon_{\alpha\beta 0\delta}q^\delta}{2M_t}T_3 + \frac{q_\alpha q_\beta}{M_t^2}T_4 \\ &\quad + \frac{g_{0\alpha}q_\beta + q_\alpha g_{0\beta}}{2M_t}T_5 \\ &\quad + i\frac{g_{0\alpha}q_\beta - q_\alpha g_{0\beta}}{2M_t}T_6 \\ &= \int d\mathbf{p} f(\mathbf{p}, \mathbf{q}) W_{\alpha\beta}(\mathbf{p}, \mathbf{q}), \end{aligned} \quad (11)$$

where $p_{\text{lab}} = (M_t, \mathbf{0})$, M_t is the mass of the target nucleus, and

$$f(\mathbf{p}, \mathbf{q}) = v_{\text{rel}}^{-1} \bar{n}_i(\mathbf{p}) [1 - n_f(\mathbf{p} + \mathbf{q})].$$

The function $\bar{n}_i(\mathbf{p})$ is the Fermi momentum distribution of the target nucleons, satisfying the normalization condition

$$\int \bar{n}_i(\mathbf{p}) d\mathbf{p} = 1.$$

The factor $1 - n_f(\mathbf{p} + \mathbf{q})$ (the unoccupation probability) takes into account the Pauli blocking for the outgoing nucleon. The relative velocity v_{rel} which represents the flux of incident particles, is given by

$$v_{\text{rel}} = |(k\mathbf{p})|/(E_\nu M_t).$$

Explicitly defining the three-momenta \mathbf{q} , \mathbf{p} , and \mathbf{p} ,

$$\begin{aligned} \mathbf{q} &= (0, 0, |\mathbf{q}|), \\ \mathbf{p} &= (\sin \theta_{\mathbf{k}}, 0, \cos \theta_{\mathbf{k}}) |\mathbf{q}|, \\ \mathbf{p} &= (\sin \theta_{\mathbf{p}} \cos \phi_{\mathbf{p}}, \sin \theta_{\mathbf{p}} \sin \phi_{\mathbf{p}}, \cos \theta_{\mathbf{p}}) |\mathbf{p}|, \end{aligned}$$

one obtains

$$v_{\text{rel}} = [E_{\mathbf{p}} - |\mathbf{p}| (\cos \theta_{\mathbf{k}} \cos \theta_{\mathbf{p}} + \sin \theta_{\mathbf{k}} \sin \theta_{\mathbf{p}} \sin \varphi_{\mathbf{p}})]/M_t,$$

where

$$E_{\mathbf{p}} = \sqrt{\mathbf{p}^2 + M^2} - \epsilon_b$$

is the total energy of the bound nucleon and ϵ_b is the effective binding energy. The angle $\theta_{\mathbf{k}}$ is defined by

$$\cos \theta_{\mathbf{k}} = \frac{E_\nu^2 + \mathbf{q}^2 + m_\ell^2}{2E_\nu |\mathbf{q}|}.$$

For determining the angle $\theta_{\mathbf{p}}$, one can use the energy conservation law defined by delta-function

$$\delta(E_{\mathbf{p}} - E_{\mathbf{p}+\mathbf{q}} + \nu) = \frac{1}{2|\mathbf{p}||\mathbf{q}|} \delta(\cos \theta_{\mathbf{p}} - \cos \theta_{\mathbf{p}}^0),$$

where $\nu = E_\nu - E_\ell$ and

$$E_{\mathbf{p}+\mathbf{q}} = \sqrt{\mathbf{p}^2 + \mathbf{q}^2 + 2|\mathbf{p}||\mathbf{q}| \cos \theta_{\mathbf{p}} + M^2}.$$

is the total energy of the outgoing nucleon. Then the condition

$$\cos \theta_{\mathbf{p}} = \cos \theta_{\mathbf{p}}^0 = \frac{(\nu + E_{\mathbf{p}})^2 - (E_{\mathbf{p}} + \epsilon_b)^2 - \mathbf{q}^2}{2|\mathbf{p}||\mathbf{q}|}$$

must be obeyed.

The nuclear structure functions are the linear combination of the W_i and can be straightforwardly calculated from Eqs. (4) and (11):

$$\begin{aligned} T_1 &= a_1 W_1 + \frac{1}{2} (a_2 - a_3) W_2, \\ T_2 &= \left[\frac{\mathbf{q}^2 - \nu^2}{2\mathbf{q}^2} (a_2 - a_3) + \frac{\nu^2}{\mathbf{q}^2} a_3 + a_4 - \frac{2\nu}{|\mathbf{q}|} a_5 \right] W_2, \\ T_3 &= \frac{M_t}{M} \left(a_7 - \frac{\nu}{|\mathbf{q}|} a_6 \right) W_3, \\ T_4 &= \frac{M_t^2}{M^2} \left[\frac{M^2}{2\mathbf{q}^2} (3a_3 - a_2) W_2 + a_1 W_4 + \frac{M}{|\mathbf{q}|} a_6 W_5 \right], \\ T_5 &= \frac{M_t}{|\mathbf{q}|} \left[\frac{\nu}{|\mathbf{q}|} (a_2 - 3a_3) + 2a_5 \right] W_2 \\ &\quad + \frac{M_t}{M} \left(a_7 - \frac{\nu}{|\mathbf{q}|} a_6 \right) W_5, \\ T_6 &= \frac{M_t}{M} \left(a_7 - \frac{\nu}{|\mathbf{q}|} a_6 \right) W_6. \end{aligned}$$

The coefficients a_i are given by

$$\begin{aligned} a_1 &= \int f(\mathbf{p}, \mathbf{q}) d\mathbf{p}, \\ a_2 &= \frac{1}{M^2} \int f(\mathbf{p}, \mathbf{q}) \mathbf{p}^2 d\mathbf{p}, \\ a_3 &= \frac{1}{M^2} \int f(\mathbf{p}, \mathbf{q}) \mathbf{p}^2 \cos^2 \theta_{\mathbf{p}} d\mathbf{p}, \\ a_4 &= \frac{1}{M^2} \int f(\mathbf{p}, \mathbf{q}) E_{\mathbf{p}}^2 d\mathbf{p}, \\ a_5 &= \frac{1}{M^2} \int f(\mathbf{p}, \mathbf{q}) E_{\mathbf{p}} |\mathbf{p}| \cos \theta_{\mathbf{p}} d\mathbf{p}, \\ a_6 &= \frac{1}{M} \int f(\mathbf{p}, \mathbf{q}) |\mathbf{p}| \cos \theta_{\mathbf{p}} d\mathbf{p}, \\ a_7 &= \frac{1}{M} \int f(\mathbf{p}, \mathbf{q}) E_{\mathbf{p}} d\mathbf{p}. \end{aligned}$$

Finally, in order to describe the neutrino scattering off a bound nucleon, one should substitute $M \mapsto M_t$ and $W_i \mapsto T_i$ in Eq. (5); then the differential cross-section can be calculated according to Eq. (2) (see Ref. [61] for more details). Table 1 collects the values of proton and neutron Fermi momenta $p_F^{p,n}$ and binding energies $\epsilon_b^{p,n}$ for several nuclei, used in our numerical calculations.

Table 1. Proton and neutron Fermi momenta and binding energies (in MeV) for selected nuclei.

Nucleus	p_F^p	ϵ_b^p	p_F^n	ϵ_b^n
$^{12}_6\text{C}$	221	25.6	221	25.6
$^{14}_7\text{N}$	223	26.2	223	26.1
$^{16}_8\text{O}$	225	26.6	225	26.6
$^{19}_9\text{F}$	233	28.4	233	28.3
$^{20}_{10}\text{Ne}$	230	27.8	230	27.8
$^{27}_{13}\text{Al}$	239	29.5	239	29.4
$^{40}_{18}\text{Ar}$	242	30.7	259	35.0
$^{56}_{26}\text{Fe}$	251	33.0	263	36.1
$^{80}_{35}\text{Br}$	245	31.5	270	38.1

4 Statistical analysis of the data

4.1 Description of experimental data

We have examined and classified all available experimental data on quasielastic scattering with $\Delta Y = 0$. Published results from the relevant experiments with ν_μ and $\bar{\nu}_\mu$ beams from accelerators at ANL [11, 12, 13, 14, 15, 16, 17, 18], BNL [19, 20, 21, 22, 23, 24, 25, 26, 27, 28, 29, 30], FNAL [31, 32, 33, 34, 35, 36, 37], CERN [38, 39, 40, 41, 42, 43, 44, 45, 46, 47, 48, 49, 50, 51, 52, 53, 54, 55, 56, 57, 58, 59, 60, 61], and IHEP [62, 63, 64, 65, 66, 67, 68, 69, 70, 71] are included dating from the end of sixties to the present day, covering a variety of nuclear targets, with energies ranging from about 150 MeV (ANL experiments) to about 350 GeV (NuTeV). Pertinent additional information was borrowed from the review articles and data compilations [95, 96, 97, 98, 99, 100, 101, 102, 103, 104, 105, 106, 107, 108, 109].

All the fits are done with the CERN function minimization and error analysis package “MINUIT” (version 94.1) [110], taking care of getting an accurate error matrix. The errors of the output parameters quoted below correspond to the usual one-standard-deviation (1σ) errors (MINUIT default).

For the analysis, we have selected the most statistically reliable measurements of the total and differential cross sections for each nuclear target, which were not superseded or reconsidered (due to increased statistics, revised normalization, etc.) in the posterior reports of the same experimental groups. Finally, we include into the global fit the data on the total cross sections from Refs. [17, 21, 22, 32, 36, 37, 40, 50, 55, 60, 61, 68, 71] and the data for the differential cross sections from Refs. [50, 57, 64, 65, 68, 71, 101]. The remaining data are either obsolete, or exhibit uncontrollable systematic errors and/or fall well outside the most probable range determined through the fit of the *full* dataset; the value of χ^2 evaluated for each subset of the rejected data usually exceeds $(3 - 4)$ NDF.

Since the differential cross sections $d\sigma/dQ^2$ were measured, as a rule, within rather wide ranges of the energy spectra of ν_μ and $\bar{\nu}_\mu$ beams, we use only the data from such experiments, in which the spectra were known (measured or calculated and then calibrated) with reasonably

good accuracy. All the energy spectra (borrowed from Refs. [50, 56, 68, 101, 104, 111, 112]) necessary for numerical averaging of the calculated differential cross sections and distributions were parametrized. To avoid the loss of accuracy, the precision of these parametrizations was chosen to be at least an order of magnitude better than the experimental accuracy of the spectra themselves. For a verification, we have estimated the mean energies of the beams for different energy intervals, and have compared these against the published values.

The analyses were performed for neutrino and antineutrino data separately, and for the full set of the ν and $\bar{\nu}$ data together. For each fit, we have included the data for either total or differential cross sections, as well as for the cross sections of both types together. The main results of the analysis are summarised in Tables 2 and 3 and illustrated in Figs. 2–19. Let us discuss these results in details.

4.2 Main results of the global fit

As is seen from Table 2, the differences between the values of M_A extracted from the fits of each type, performed with the BBBA(07) and GKex(05) models for the vector form factors vary between 0.3% and 1.3% that is less than or of the order of one standard deviation in the M_A extractions and is comparable with the accuracy of the most precise measurements of the electric and magnetic form factors. The values of χ^2/NDF are essentially the same for BBBA(07) and GKex(05). The differences in the M_A values obtained with the two versions of the BBBA(07) model corresponding to $d/u = 0$ and 0.2 (the latter is not shown in the table) are less than 0.2% that is practically negligible. Therefore, in the following we will solely discuss the $d/u = 0$ case.

The M_A values obtained from the fits to the differential cross sections are systematically lower those obtained from the total cross sections. The differences amount $\sim 1.5\%$ ($\sim 5.7\%$) for ν_μ ($\bar{\nu}_\mu$) that is (especially in antineutrino case) above the statistical error of the fit and is caused mainly by uncertainties in the energy spectra of ν_μ and $\bar{\nu}_\mu$ and, in lesser extent, in the nuclear effects.

Figures 2 and 3 show a compilation of the available data on the total QES cross sections for the following nuclear targets: hydrogen [21], deuterium [14, 15, 16, 17, 22, 32, 57], carbon [61], aluminium [63, 65, 67, 68], argon [60], iron [37], steel [12], propane [43], freon [40, 45, 48, 50, 62, 70, 71, 104], and also propane–freon [52, 55, 56] and neon–hydrogen [33, 34, 36] mixtures. The recent MiniBooNE 2007 datapoint [5] (carbon target) estimated from the reported value of M_A is also shown in Fig. 2 for comparison.

The compilation does not include obviously obsolete data (e.g., ANL 1972 [13], CERN HLBC 1965/1966 [38, 39]), as well as the data identical to those reported in the posterior publications of the same experimental groups (e.g., FNAL 1982 [31], GGM 1978 [53], IHEP-ITEP 1983 [66], IHEP SKAT 1986 [69]). The early results of the NOMAD experiment reported in Refs. [58, 59], have been considerably revised (mainly due to corrections in nuclear Monte Carlo) [61]; the datapoints shown in Fig. 2 are still

Table 2. Values of M_A (given in GeV), extracted by fitting the ν_μ , $\bar{\nu}_\mu$, and $\nu_\mu + \bar{\nu}_\mu$ data on total and differential QES cross sections, using the BBBA(07) and GKex(05) models for the vector form factors of the nucleon. The χ^2/NDF values for each fit are shown in parentheses.

BBBA(07)			GKex(05)		
M_A^ν	$M_A^{\bar{\nu}}$	$M_A^{\nu+\bar{\nu}}$	M_A^ν	$M_A^{\bar{\nu}}$	$M_A^{\nu,\bar{\nu}}$
Fit to the total cross sections:					
0.994 ± 0.017 (83/82)	1.047 ± 0.025 (134/62)	1.011 ± 0.014 (220/145)	0.986 ± 0.017 (83/82)	1.035 ± 0.025 (137/62)	1.001 ± 0.014 (222/145)
Fit to the differential cross sections:					
0.979 ± 0.020 (45/48)	0.991 ± 0.029 (26/37)	0.983 ± 0.017 (71/86)	0.976 ± 0.020 (45/48)	0.982 ± 0.030 (25/37)	0.978 ± 0.017 (70/86)
Fit to the total and differential cross sections:					
0.988 ± 0.013 (128/131)	1.023 ± 0.018 (163/100)	0.999 ± 0.011 (293/232)	0.981 ± 0.013 (128/131)	1.012 ± 0.019 (163/100)	0.991 ± 0.011 (293/232)

preliminary and are reproduced here by permission of the NOMAD Collaboration.

All the deuterium data quoted in Fig. 2 and freon data in Fig. 3 were converted to a free nucleon target by the experimenters.⁴ The BNL 1981 experiment [22] had reported the E_ν and Q^2 dependencies of M_A extracted from a fit of the experimental Q^2 distribution rather than the cross section; we quote the BNL 1981 cross section recalculated from M_A by Kitagaki et al. [32]. Similarly, the FNAL 1984 rectangle [33,34] and FNAL 1987 datapoint [36] were calculated by the experimenters (for free proton target) using the M_A value extracted from the measured Q^2 distribution of $\bar{\nu}_\mu$ events recorded in the Fermilab 15' bubble chamber filled with a heavy neon-hydrogen mixture. The data from several freon experiments (e.g., [40, 45, 97]) reported in the original papers in units cm^2 per nucleon of freon nucleus, were converted to the standard units.

All solid curves shown in the figures were calculated using the BBBA(07) model for vector form factors with $d/u = 0$ and always correspond to the best fit value

$$M_A^{\nu+\bar{\nu}} = 0.999 \pm 0.011 \text{ GeV} \quad (\chi^2/\text{NDF} \approx 1.3) \quad (12)$$

obtained from the global fit of neutrino and antineutrino data on the total and differential cross sections (see Table 2). We do not show the cross sections calculated with the GKex(05) model since the difference will be practically invisible.

The dashed curves in Fig. 2 are calculated with the M_A values extracted from the best fit to the (preliminary) NOMAD total cross section data alone [61]:

$$\begin{aligned} M_A^\nu &= 1.05 \pm 0.02_{\text{stat}} \pm 0.07_{\text{syst}} \text{ GeV}, \\ M_A^{\bar{\nu}} &= 1.06 \pm 0.07_{\text{stat}} \pm 0.12_{\text{syst}} \text{ GeV}, \end{aligned} \quad (13)$$

⁴ The nuclear corrections applied to the deuterium data under consideration, were treated according to Singh [113]. The nuclear effects for the freon data were modeled using a Fermi gas approach.

both agree with the global fit value (12). Note that these results were obtained with the GKex(05) vector form factors. Fitting the NOMAD data with the BBBA(07) form factors increases M_A^ν and $M_A^{\bar{\nu}}$ by about 0.8 and 0.9%, respectively, that still remains well within the errors quoted in (13).

As is seen from the figures, the obtained result, despite the non-optimal χ^2 and large spread of the data, is not in conflict with the main part of the data excluded from the global fit. Moreover, it well agrees with the world averaged value of

$$M_A = 1.014 \pm 0.014 \text{ GeV}, \quad (14)$$

obtained in Ref. [3] as a result of their reanalysis of the “raw” data from $\nu_\mu d$ and $\bar{\nu}_\mu H$ experiments ANL 1973 [14], ANL 1977 [17], ANL 1982 [18], BNL 1980 [21], BNL 1981 [22], BNL 1983 [114], BNL 1990 [28], FNAL 1983 [32], CERN BEBC 1990 [57], and from pion electroproduction experiments after corrections for hadronic effects. Note that the values of M_A re-extracted in Ref. [3] from each $\nu_\mu d$ experiment separately spread between 0.97 ± 0.05 and 1.04 ± 0.06 GeV. It exceeds the difference between the results of our analysis of data on total and differential cross sections. Both analyses use the same BBBA(07) model and mutually supplement each other, since they practically do not overlap in the adopted data sets. Formal averaging of the values (12) and (14) yields

$$M_A = 1.006 \pm 0.009 \text{ GeV}.$$

4.3 Are M_A^ν and $M_A^{\bar{\nu}}$ really different?

According to the global fit (see Table 2), the difference between the values of M_A^ν and $M_A^{\bar{\nu}}$ obtained by fitting the neutrino and antineutrino data separately, reaches about 3.5% for BBBA(07) and about 3.2% for GKex(05) that is above the statistical error in determination of M_A^ν and $M_A^{\bar{\nu}}$. However, taking into account the systematic difference between the fits of total and differential cross section

data, as well as high values of χ^2/NDF , this difference cannot be considered statistically significant. Furthermore, the fit to the antineutrino data is not stable relative to including/excluding some data subsets. In particular, as is seen from Fig. 2, the total NuTeV cross sections per nucleon bound in iron, averaged over the energy range $E_{\nu,\bar{\nu}} = 30 \div 300$ GeV

$$\begin{aligned}\bar{\sigma}(\nu_\mu n \rightarrow \mu^- p) &= (0.94 \pm 0.03_{\text{stat}} \pm 0.07_{\text{syst}}) \times 10^{-38} \text{ cm}^2, \\ \bar{\sigma}(\bar{\nu}_\mu p \rightarrow \mu^+ n) &= (1.12 \pm 0.04_{\text{stat}} \pm 0.10_{\text{syst}}) \times 10^{-38} \text{ cm}^2\end{aligned}$$

(shown in Fig. 2 by rectangles) notably exceed the corresponding best fit curves whereby the NuTeV data [37] strongly affects the global fit values of M_A^ν and $M_A^{\bar{\nu}}$.

To clarify this point further, we have performed additional fits, in which the datasets obtained in experiments with non-active targets have been removed. Namely, we excluded the highest energy NuTeV total cross section data (iron target) [37] and the data on differential cross sections measured with the IHEP-ITEP spark chamber detector with aluminium filters [63,65,68], since these experiments do not have an active target to measure recoil hadrons and surely remove resonance background. In order to minimize possible uncertainties in nuclear corrections, the lowest-energy CERN 1967 total cross section data (freon target) [40] were also excluded from these fits. The results of this analysis are summarized in Table 3. It is seen that the additional reduction of the dataset essentially *decreases* the resulting values of M_A . Concurrently it improves the statistical quality of the fits to the total cross section data, while slightly increases the χ^2/NDF for the fit to the differential cross sections. Besides that, the M_A values extracted from the total and differential cross sections become bit more consistent. The differences between M_A^ν and $M_A^{\bar{\nu}}$ [-65 MeV for BBBA(07) and -75 MeV for GKex(05)] become *opposite in sign* to those obtained from our “default” fit performed with the full dataset. However, both M_A^ν and $M_A^{\bar{\nu}}$ values are still compatible, within the 1σ deviation, with the average value of $M_A^{\nu+\bar{\nu}}$. So we may reckon that

- (i) the axial mass extraction is rather responsive to the choice of the data subsets and
- (ii) the current experimental data cannot definitely confirm or disconfirm possible difference between the axial masses extracted from experiments with neutrino and antineutrino beams.

Similar fit performed for the differential cross section data only, from which all the $\nu_\mu d$ data were excluded, leads to an *increase* of M_A^ν by about 4.2% (4.4%) for BBBA(07) (GKex(05)). However, the statistical error of this fit increases too. Including into this fit the non-deuterium data on total cross sections diminish the increase of M_A^ν to about 1.2% for both BBBA(07) and GKex(05). Hence, the above conclusions remain essentially unchanged.

4.4 Further details on differential cross section data

As is known from the comparison with the low-energy electron-nucleus scattering data, the RFG description of

the low- Q^2 region is not enough accurate especially at energies below ~ 2 GeV (for recent discussion, see, e.g., Refs. [115,116] and references therein). Moreover, the shape of $d\sigma/dQ^2$ at $Q^2 \lesssim 0.1$ GeV² is slowly sensitive to variations of M_A (see below). Thus, in order to minimize possible uncertainties due to nuclear effects, the points with $Q^2 < 0.15$ GeV² were rejected from the fit of the differential cross section dataset. Leaving these points in the fit would lead to a *decrease* of the output values of M_A^ν , $M_A^{\bar{\nu}}$, and $M_A^{\nu,\bar{\nu}}$ obtained from the $d\sigma/dQ^2$ dataset by, respectively, 1.8, 3.3, and 2.2% for BBBA(07) and 2.0, 4.0, and 2.6% for GKex(05) form factors. The corresponding decrease of M_A derived from the full dataset (σ and $d\sigma/dQ^2$) is clearly less essential: respectively, 0.7, 1.3, and 0.9% for BBBA(07) and 0.7, 1.5, and 1.0% for GKex(05).

Of course, the mentioned uncertainty still remains in the RFG calculations of the total cross sections, since the contribution from the low- Q^2 region is essential at low energies. To illustrate this, we show in Fig. 4 the relative contribution of the region $Q^2 < Q_1^2$ into the total cross section, $R(Q_1^2) = \sigma(Q^2 < Q_1^2)/\sigma$, as a function of Q_1^2 , evaluated for ν_μ and $\bar{\nu}_\mu$ QE interactions with carbon at several (anti)neutrino energies using $M_A = 1$ GeV.⁵ It is seen that for neutrino-nucleus interactions $R \lesssim 0.25$ as $Q_1^2 < 0.15$ GeV² and $E_\nu > 0.7$ GeV that is for all energies of our current interest. As a result, a few percent error expected in $d\sigma/dQ^2$ due to inaccuracy of the RFG model for the low- Q^2 region, becomes nearly negligible in the total cross section. However it is not the case for antineutrino interactions, for which the ratio $R(Q_1^2 = 0.15 \text{ GeV}^2)$ becomes reasonably small ($R \lesssim 0.3$) only for $E_\nu \gtrsim 2$ GeV. Therefore the lower energy antineutrino total cross section data may bias an uncontrolled (while still small) additional uncertainty. Fortunately, the major part of the data participated in the global fit satisfies the above conditions and our examination demonstrates that the related uncertainty is not weighty.

Figures 5–7 (a) and 8–11 represent the spectrum-averaged differential cross sections for several nuclear targets: deuterium (Fig. 5) [57], aluminium (Figs. 6 and 7 (a)) [63, 65,68], freon (Figs. 8, 9 and 10) [50,70,71,101,104], and propane-freon mixture (Fig. 11) [55,52]. In Fig. 7 (b) we show (for illustrative purposes only) the axial-vector form factor extracted in the IHEP-ITEP spark chamber experiment [68]. All the quoted data, except those from Ref. [70] (superseded by the data from the more recent publication by the SKAT Collaboration [71]), model-dependent IHEP-ITEP data on $F_A(Q^2)$ [68], and a few rejected low- Q^2 datapoints, participate in the global fit. We show the cross sections calculated with M_A obtained by individual fits to the data of each experiment alone and compare these against the cross sections evaluated with the global-fit value of M_A . All the details are recounted in the captions and legends of the figures. The comparison demonstrates that the individual and global fits generally

⁵ Here $\sigma(Q^2 < Q_1^2)$ is defined as an integral of $d\sigma/dQ^2$ from the kinematical minimum of Q^2 to $Q^2 = Q_1^2$.

Table 3. The same as in Table 2 but after exclusion of the datasets from experiments with non-active targets (NuTeV 1984 [37], IHEP-ITEP 1981,82,85 [63,65,68]) and the lowest-energy data of CERN 1967 [40] (see text for details).

BBBA(07)			GKex(05)		
M_A^ν	$M_A^{\bar{\nu}}$	$M_A^{\nu+\bar{\nu}}$	M_A^ν	$M_A^{\bar{\nu}}$	$M_A^{\nu,\bar{\nu}}$
Fit to the total cross sections:					
0.986 ± 0.021 (42/52)	0.855 ± 0.046 (38/35)	0.958 ± 0.019 (88/88)	0.977 ± 0.021 (42/52)	0.837 ± 0.046 (38/35)	0.948 ± 0.019 (89/88)
Fit to the differential cross sections:					
0.966 ± 0.024 (33/33)	0.971 ± 0.042 (16/22)	0.967 ± 0.021 (49/56)	0.963 ± 0.024 (34/33)	0.959 ± 0.043 (15/22)	0.962 ± 0.021 (49/56)
Fit to the total and differential cross sections:					
0.977 ± 0.016 (75/86)	0.912 ± 0.030 (58/58)	0.962 ± 0.014 (137/145)	0.971 ± 0.016 (76/86)	0.896 ± 0.031 (57/58)	0.954 ± 0.014 (138/145)

do not contradict each other. The differences are within the experimental errors and are not of systematic nature.

As a further test of the global fit, we show in Fig. 12 the flux-weighted differential cross sections $d\sigma(\nu_\mu n \rightarrow \mu^- p)/dy$ and $d\sigma(\bar{\nu}_\mu p \rightarrow \mu^+ n)/dy$ (divided by energy), which were measured with the Gargamelle bubble chamber filled with liquid freon and exposed to the wide-band CERN-PS ν_μ and $\bar{\nu}_\mu$ beams. Several analyses of these data samples are available from the literature (see Refs. [46, 47, 49, 101] and also Ref. [105] for a review). Figure 12 shows two representative versions taken from Refs. [47] and [101] – the preliminary and final results of the GGM experiment, respectively. The data are shown for the five narrow instrumental ranges: 1 – 2, 2 – 3, 3 – 5, 5 – 11, and 5 – 20 GeV. The measured cross sections were converted from freon to a free nucleon target by the experimenters, after accounting for Fermi motion of the nucleons and Pauli suppression of quasielastic events.

For a qualitative comparison, we have performed individual fits to the GGM data, separately for neutrino and antineutrino differential cross sections. In order to reduce possible error introduced by RFG calculations of nuclear effects, the energy range of 1 – 2 GeV has been excluded from this likelihood analysis. As is seen from the figure, the M_A value extracted from the neutrino subsample does not contradict to that from the global fit, while it is not so for the antineutrino data subsample where the discrepancy is essential. This discrepancy can be attributed (at least, partially) to the vagueness of the model for nuclear effects used in the analyses of the GGM data. Since the details of the GGM nuclear Monte Carlo are not available, we do not include this data sample into the global fit. We note, however, that the inclusion of these data (also without the low-energy datapoints) into the fit only leads to a small *decrease* of the output values of M_A^ν , $M_A^{\bar{\nu}}$, and $M_A^{\nu,\bar{\nu}}$ – by, respectively, 0.4, 2.2, and 0.9% for BBBA(07) and 0.3, 2.0, and 0.8% for GKex(05) form factors. The corresponding χ^2/NDF values remain nearly the same.

4.5 Q^2 distributions

An additional fruitful set of available data is the Q^2 distributions dN/dQ^2 of the QES events measured in several experiments with different nuclear targets. Usually just dN/dQ^2 is considered as the observable most appropriate for extracting axial mass value, since it is less dependent of the flux and spectrum uncertainties in comparison with the differential or total cross sections. However, in comparison with the differential cross section, the Q^2 distribution has two drawbacks: it contains an uncertainty due to normalization, and it is generally less responsive to variations of M_A at high Q^2 . Figure 13 illustrates the second point. It shows the Q^2 distributions and differential cross sections for ν_μ and $\bar{\nu}_\mu$ quasielastic scattering off free nucleons, evaluated with different values of M_A and normalized to the corresponding quantities calculated with $M_A = 1$ GeV. The calculations are done with the fixed values of energy corresponding to the mean (anti)neutrino beam energies in experiments [34, 43, 56, 62]. It is seen from the figure that the region $Q^2 \lesssim 0.15$ GeV² strongly affected by the nuclear effects, is sensitive to M_A for dN/dQ^2 and less sensitive for $d\sigma/dQ^2$; the situation is opposite for the high Q^2 region for which the nuclear corrections are less important.

We use the measured Q^2 distributions for a consistency test of our analysis. For illustration, we show the four sets of data on Q^2 distributions measured in experiments HLBC 1969 (propane) [43] (Fig. 14), IHEP SKAT 1981 (freon) [62] (Fig. 15), CERN GGM 1979 (propane–freon mixture) [56] (Fig. 16), and FNAL E180 (neon–hydrogen mixture) [33, 34] (Fig. 17). The curves shown in the figures are calculated with the global-fit M_A and normalized to the data after fitting of the normalization factor N . The shaded bands indicate the uncertainty due mainly to indetermination of this factor. The obtained best-fit values of N should be compared with these evaluated directly from the experimental data (all values are shown in the legends of the figures). One can see that the agreement is excellent everywhere. So, we may conclude that this test was quite successful.

Another important confirmation of our result is a reasonably good agreement with the M_A value extracted in our earlier analysis of the data on total inelastic $\nu_\mu N$ and $\bar{\nu}_\mu N$ CC cross sections and relevant observables [117].

Finally, Fig. 18 presents a comparison of the total QES cross sections for ν_e , ν_μ , ν_τ , $\bar{\nu}_e$, $\bar{\nu}_\mu$, and $\bar{\nu}_\tau$ interactions with free nucleons, calculated with the obtained best-fit value of $M_A = 0.999 \pm 0.011$ GeV by using the BBBA(07) model of vector form factors. The shaded bands reproduce the uncertainty due to the 1σ error in M_A .

5 Discussion and conclusions

We performed a statistical study of the QES total and differential cross section data in order to extract the best-fit values of the parameters M_A . Our main results are summarized in Table 2 are, of course, model dependent and can be recommended for use only within the same (or numerically equivalent) model assumptions as in the present analysis. The best-fit values of the axial mass obtained by different fits do not contradict to each other and agree with the recent re-extraction of M_A from $\nu_\mu d$, $\bar{\nu}_\mu H$, and pion electroproduction experiments, reported in Ref. [3]. They are also in agreement with the *preliminary* result of high-statistical NOMAD experiment at CERN, as well as with the numerous earlier data which were not included into the likelihood analysis. It has been demonstrated that removing the data subsets obtained in experiments with non-active targets, particularly the NuTeV dataset, leads to a further *decrease* of the extracted values of M_A (see Table 3). In other words, there is no way to increase the M_A value which follows from essentially all (anti)neutrino data on total and differential QES cross sections.

On the other hand, our best-fit value of M_A is in a conflict with the mean values of M_A reported by K2K and MiniBooNE Collaborations [4, 5], even after accounting for the maximum possible systematic error of our analysis related primarily to its susceptibility to the choice of the data subsets. To expound the problem, let us consider the representative K2K result with more details.

The M_A value reported in Ref. [4] has been obtained with a water target by fitting the Q^2 distributions of muon tracks reconstructed from neutrino-oxygen quasielastic interactions by using the combined K2K-I and K2K-IIa data from the Scintillating Fiber detector (SciFi) in the KEK accelerator to Kamioka muon neutrino beam. The experimental data from the continuation of the K2K-II period were not used in the analysis of Ref. [4]. The best-fit values of M_A obtained from the K2K-I and K2K-IIa data subsets separately are, respectively, 1.12 ± 0.12 GeV ($\chi^2/\text{NDF} = 150/127$) and 1.25 ± 0.18 GeV ($\chi^2/\text{NDF} = 109/101$).

Figure 19 shows the $\nu_\mu n \rightarrow \mu^- p$ total cross section per neutron bound in oxygen, recalculated from the fitted values of M_A derived in Ref. [4] from the Q^2 distribution shape for each reconstructed neutrino energy. It is necessary to underline here that the authors do not consider their result for each energy bin as a *measurement*, but rather a *consistency test*. All calculations represented in Fig. 19 were done with our default inputs that introduces

an uncertainty of at most 2%; this uncertainty is added quadratically to the quoted error bars. Also shown are the cross sections evaluated by using our best fit value (12), the K2K value of 1.20 ± 0.12 GeV, and the value of 1.1 GeV used as a default in the recent neutrino oscillation analyses to the data from K2K [118, 119] and Super-Kamiokande I [120]. A significant systematic discrepancy is clearly seen at $E_\nu > 1$ GeV. Since the energy region covered by the K2K analysis extends to about 4 GeV, it seems problematic to explain this discrepancy by the inapplicability of the RFG model alone.

Considering that the low-energy K2K and MiniBooNE data are in agreement with each other and do not contradict to the high-energy NuTeV results, we may conclude that the new generation experiments for studying the quasielastic neutrino and antineutrino interactions with nucleons and nuclei are of urgent necessity, in order to resolve the inconsistencies between the old and new measurements of the axial-vector mass.

6 Acknowledgements

This study is currently supported by the Russian Foundation for Basic Research under Grant No. 07-02-00215-a. The authors would like to thank Krzysztof M. Graczyk, Sergey A. Kulagin, Dmitry V. Naumov, Jan T. Sobczyk, and Oleg V. Teryaev for helpful discussions. We thank the NOMAD Collaboration for permission to use their data prior to publication and Antonio Bueno for explaining us some points of LAr TPC experiment. We are especially grateful to Arie Bodek for his constructive comments and suggestions. V. V. L. is very thankful to LPNHE (Paris) for warm hospitality and financial support during a stage of this work.

References

1. A. Liesenfeld et al., “A measurement of the axial form factor of the nucleon by the $p(e, e'\pi^+)n$ reaction at $W = 1125$ MeV,” Phys. Lett. B **468**, 20 (1999) [arXiv:nucl-ex/9911003]
2. V. Bernard, L. Elouadrhiri, Ulf-G. Meißner, “Axial structure of the nucleon: Topical review,” J. Phys. G **28**, R1 (2002) [arXiv:hep-ph/0107088]
3. A. Bodek, S. Avvakumov, R. Bradford, H. Budd, “Extraction of the axial nucleon form factor from neutrino experiments on deuterium,” arXiv:0709.3538 [hep-ex]
4. R. Gran et al. (K2K Collaboration), “Measurement of the quasi-elastic axial vector mass in neutrino oxygen interactions,” Phys. Rev. D **74**, 052002 (2006) [arXiv:hep-ex/0603034]
5. A. A. Aguilar-Arevalo et al. (MiniBooNE Collaboration), “Measurement of muon neutrino quasi-elastic scattering on carbon,” Phys. Rev. Lett. **100**, 032301 (2008) [arXiv:0706.0926 [hep-ex]]
6. T. Katori (for the MiniBooNE Collaboration), “Charged-current interaction measurements in Mini-BooNE,” AIP Conf. Proc. **967**, 123 (2007) [arXiv:0709.4498 [hep-ex]]

7. P. E. Bosted, “An Empirical fit to the nucleon electromagnetic form-factors,” *Phys. Rev. C* **51**, 409 (1995)
8. H. Budd, A. Bodek, J. Arrington, “Modeling quasi-elastic form factors for electron and neutrino scattering,” arXiv:hep-ex/0308005
9. R. Bradford, A. Bodek, H. Budd, J. Arrington, “A new parameterization of the nucleon elastic form factors,” *Nucl. Phys. B Proc. Suppl.* **159**, 127 (2006) [arXiv:hep-ex/0602017]
10. R. A. Smith, E. J. Moniz, “Neutrino reactions on nuclear targets,” *Nucl. Phys. B* **43**, 605 (1972); erratum – *ibid.* **101**, 547 (1975)
11. T. B. Novey, “II. Quasi-elastic neutrino interactions,” *Proc. Roy. Soc. Lond. A* **301**, 113 (1967)
12. R. L. Kustom et al., “Quasielastic neutrino scattering,” *Phys. Rev. Lett.* **22**, 1014 (1969)
13. W. A. Mann et al., “Study of the reaction $\nu + n \rightarrow \mu^- + p$,” in: Proceedings of the 16th International Conference on High Energy Physics, National Accelerator Laboratory, Chicago-Batavia, Illinois, September 6–13, 1972, ed. by J. D. Jackson, A. Roberts (National Accelerator Laboratory, Batavia, Illinois, 1973), paper #784
14. W. A. Mann et al., “Study of the reaction $\nu + n \rightarrow \mu^- + p$,” *Phys. Rev. Lett.* **31**, 844 (1973)
15. S. J. Barish et al. (ANL-Purdue Collaboration), “An inclusive look at νp and νn charged-current reactions below 6 GeV,” preprints COO-1428-428, ANL-HEP-CP-75-38 (unpublished)
16. R. A. Singer, “Study of the reaction $\nu + n \rightarrow \mu^- + p$,” in: Proceedings of the International Conference on Neutrino Physics and Astrophysics, “Neutrino’77,” Baksan Valley, USSR, June 18–24, 1977, ed. by M. A. Markov, G. V. Domogatsky, A. A. Komar, A. N. Tavkhelidze (Publishing office “Nauka,” Moscow, USSR, 1978), Vol. **2**, p. 95
17. S. J. Barish et al., “Study of neutrino interactions in hydrogen and deuterium: description of the experiment and study of the reaction $\nu + d \rightarrow \mu^- + p + p_s$,” *Phys. Rev. D* **16**, 3103 (1977)
18. K. L. Miller et al., “Study of the reaction $\nu + d \rightarrow \mu^- + p + p_s$,” *Phys. Rev. D* **26**, 537 (1982)
19. E. G. Cazzoli et al., “Quasi-elastic neutrino scattering and the axial vector form factor,” in: Proceedings of the International Neutrino Conference, Aachen, West Germany, June 8–12 1976, ed. by H. Faissner, H. Reithler, P. Zerwas (Vieweg, 1977), p. 405; see also preprint BNL-21677, NG-349, Brookhaven National Laboratory, 1976 (unpublished)
20. A. M. Cnops et al., “Neutrino-deuterium reactions in the 7-foot bubble chamber,” in: Proceedings of the Topical Conference on Neutrino Physics at Accelerators, Oxford, England, July 4–7, 1978, ed. by A. G. Michette, P. B. Renton (Rutherford Lab, 1978), p. 62; see also preprint BNL-24848, OG431, Brookhaven National Laboratory, 1978 (unpublished)
21. G. Fanourakis et al., “Study of low-energy antineutrino interactions on protons,” *Phys. Rev. D* **21**, 562 (1980)
22. N. J. Baker et al., “Quasielastic neutrino scattering: A measurement of the weak nucleon axial-vector form factor,” *Phys. Rev. D* **23**, 2499 (1981)
23. T. Kitagaki et al., “Charged-current exclusive pion production in neutrino-deuterium interactions,” *Phys. Rev. D* **34**, 2554 (1986)
24. T. Kitagaki et al., “Comparison of quasielastic scattering $\nu_{\mu}n \rightarrow \mu^-p$ and Δ^{++} production reaction $\nu_{\mu}p \rightarrow \mu^- \Delta^{++}$ in the BNL 7-ft deuterium bubble chamber,” in: Proceedings of the International 12th Conference on Neutrino Physics and Astrophysics, “Neutrino’86,” Sendai, Japan, June 3–8, 1986, ed. by T. Kitagaki, H. Yuta (World Scientific, 1987), p. 525; see also preprints BNL-39020 and CONF-8606201-6, 1986 (unpublished)
25. K. Abe et al., “Precise determination of $\sin^2 \theta_W$ from measurements of the differential cross sections for $\nu_{\mu}p \rightarrow \nu_{\mu}p$ and $\bar{\nu}_{\mu}p \rightarrow \bar{\nu}_{\mu}p$,” *Phys. Rev. Lett.* **56**, 1107 (1986)
26. L. A. Ahrens et al., “Measurement of neutrino-proton and antineutrino-proton elastic scattering,” *Phys. Rev. D* **35**, 785 (1987)
27. L. A. Ahrens et al., “A study of the axial-vector form factor and second-class currents in antineutrino quasi-elastic scattering,” *Phys. Lett. B* **202**, 284 (1988)
28. T. Kitagaki et al., “Study of $\nu d \rightarrow \mu^- pp_s$ and $\nu d \rightarrow \mu^- \Delta^{++}(1232)n_s$ using the BNL 7-foot deuterium-filled bubble chamber,” *Phys. Rev. D* **42**, 1331 (1990)
29. M. Sakuda, “Study of neutrino-nucleus interactions for neutrino oscillations,” in: Proceedings of the 4th International Workshop on Neutrino Oscillations and Their Origin (“NOON 2003”), Kanazawa, Japan, February 10–14, 2003, ed. by Y. Suzuki, M. Nakahata, M. Shiozawa, Y. Obayashi (River Edge, World Scientific, 2004), p. 253
30. K. Furuno et al., “BNL 7-foot bubble chamber experiment – neutrino deuterium interactions,” a talk at the 2nd International Workshop on Neutrino-Nucleus Interactions in the few-GeV Region, NuInt’02,” University of California, Irvine, December 12–15, 2002, RCNS-03-01, KEK Preprint 2003-48, September, 2003 (unpublished)
31. A. E. Asratyan et al., “Antineutrino quasielastic scattering in neon and total cross section for charged current interactions in the energy range 10 to 50 GeV,” in: Proceedings of the 12th International Neutrino Conference “Neutrino’82,” Balatonfüred, Hungary, June 14–19, 1982, ed. by A. Frenkel, L. Jenik (Central Research Institute of Physics, Budapest, 1982), Supplement Vol. **2**, p. 139
32. T. Kitagaki et al., “High-energy quasielastic $\nu_{\mu}n \rightarrow \mu^-p$ scattering in deuterium,” *Phys. Rev. D* **28**, 436 (1983)
33. A. E. Asratyan et al., “Antineutrino quasielastic scattering in neon and total cross sections in the energy interval 10–50 GeV,” *Yad. Fiz.* **39**, 619 (1984) [*Sov. J. Nucl. Phys.* **39**, 392 (1984)]
34. A. E. Asratyan et al., “Total antineutrino–nucleon charged current cross section in the energy range 10–50 GeV,” *Phys. Lett.* **137B**, 122 (1984)
35. V. V. Ammosov et al., “Quasielastic production of Λ hyperon in antineutrino interactions at high energies,” *Pisma Zh. Eksp. Teor. Fiz.* **43**, 554 (1986) [*JETP Lett.* **43**, 716 (1986)]
36. V. V. Ammosov et al. (IHEP-ITEP-MPEI Collaboration), “Neutral strange particle exclusive production in charged current high-energy antineutrino interactions,” *Z. Phys. C* **36**, 377 (1987)
37. N. Suwonjandee, “The measurement of the quasi-elastic neutrino-nucleon scattering cross section at the Tevatron,” Ph.D. Thesis, University of Cincinnati, Cincinnati, 2004, FERMLAB-THESIS-2004-67, Fermi Na-

- tional Accelerator Laboratory, Illinois, 2004 (unpublished); UMI 31-20857
38. H. Burmeister et al., “Further analysis of the neutrino interactions in the CERN heavy liquid bubble chamber,” in: Proceedings of the Informal Conference on Experimental Neutrino Physics, CERN, Geneva, January 20–22, 1965, ed. by C. Franzinetti, CERN Yellow Report No. 65-32, European Organization for Nuclear Research, Geneva, 1965, p. 25
 39. C. Franzinetti, “Neutrino interactions in the CERN heavy liquid bubble chamber,” Lecture given at the Chicago Meeting of the American Physical Society, Chicago, October 28, 1965, CERN Yellow Report No. 66-13, European Organization for Nuclear Research, Geneva, March 1966 (unpublished)
 40. E. C. M. Young, “High-energy neutrino interactions,” Ph.D. Thesis, CERN Yellow Report No. 67-12, European Organization for Nuclear Research, Geneva, 1967 (unpublished)
 41. A. Orkin-Lecourtois, C. A. Piketty, “The quasi-elastic events of the CERN bubble chamber neutrino experiment and determination of the axial form factor,” *Nuovo Cim.* **50 A**, 927 (1967)
 42. M. Holder et al., “Spark-chamber study of elastic neutrino interactions,” *Nuovo Cim.* **57 A**, 338 (1968)
 43. I. Budagov et al., “A study of the elastic neutrino process $\nu + n \rightarrow \mu^- + p$,” *Lett. Nuovo Cim.* **2**, 689 (1969)
 44. T. Eichten et al., “Observation of “elastic” hyperon production by antineutrinos,” *Phys. Lett.* **40 B**, 593 (1972)
 45. T. Eichten et al., “Measurement of the neutrino–nucleon and antineutrino–nucleon total cross sections,” *Phys. Lett.* **46 B**, 274 (1973)
 46. F. J. Sciulli, “Total and differential cross-sections in deep inelastic neutrino scattering,” in: Proceedings of the 4th International Conference on Neutrino Physics and Astrophysics “Neutrino’74,” Dornigtown, Pennsylvania, April 26–28, 1974, ed. by Ch. Baltay, AIP Conf. Proc. **22**, 166 (1974)
 47. M. Hagnauer (for the Aachen-Brussels-CERN-Paris-Milano-Orsay-London Collaboration), “‘Gargamelle’ experiment,” in: Proceedings of the 17th International Conference on High Energy Physics, London, July 1–10, 1974, ed. by J. R. Smith (Rutherford High Energy Laboratory, Didcot, Berkshire, England, 1975), p. IV-95
 48. M. Rollier (for the Aachen-Bruxelles-CERN-Ecole Polytechnique-Orsay-London Collaboration), “Elastic neutrino and antineutrino interactions,” in: Proceedings of the International Colloquium on High Energy Neutrino Physics, Paris, France, March 18–20, 1975, (Editions du CNRS, École Polytechnique, 1975), p. 349
 49. H. Deden et al. (Gargamelle Neutrino Collaboration), “Experimental study of structure functions and sum rules in charge-changing interactions of neutrinos and antineutrinos on nucleons,” *Nucl. Phys. B* **85**, 269 (1975)
 50. S. Bonetti et al., “Study of quasielastic reactions of neutrino and antineutrino in Gargamelle,” *Nuovo Cim.* **38 A**, 260 (1977)
 51. O. Erriquez et al., “Strange particle production by antineutrinos,” *Phys. Lett.* **70 B**, 383 (1977)
 52. M. Rollier (for the Gargamelle Antineutrino Collaboration, Bari-Milano-Strasbourg-Torino-University College London), “Recent results from the Gargamelle $\bar{\nu}$ propane experiment at the CERN-PS,” in: Proceedings of the Topical Conference on Neutrino Physics at Accelerators, Oxford, England, July 4–7, 1978, ed. by A. G. Michette, P. B. Renton (Rutherford Lab, 1978), p. 68
 53. M. Dewit (for the Aachen-Bruxelles-CERN-Ecole Polytechnique-Orsay-Padova Collaboration), “Experimental study of the reaction $\nu n \rightarrow \mu^- p$,” in: Proceedings of the Topical Conference on Neutrino Physics at Accelerators, Oxford, England, July 4–7, 1978, ed. by A. G. Michette, P. B. Renton (Rutherford Lab, 1978), p. 75
 54. O. Erriquez et al., “Production of strange particles in antineutrino interactions at the CERN PS,” *Nucl. Phys. B* **140**, 123 (1978)
 55. M. Pohl et al. (Gargamelle Neutrino Propane Collaboration), “Experimental study of the reaction $\nu n \rightarrow \mu^- p$,” *Lett. Nuovo Cim.* **26**, 332 (1979)
 56. N. Armenise et al., “Charged current elastic antineutrino interactions in propane,” *Nucl. Phys. B* **152**, 365 (1979)
 57. D. Allasia et al. (Amsterdam-Bergen-Bologna-Padova-Pisa-Saclay-Torino Collaboration), “Investigation of exclusive channels in $\nu/\bar{\nu}$ -deuteron charged current interactions,” *Nucl. Phys. B* **343**, 285 (1990)
 58. R. Petti (for the NOMAD Collaboration), “Precision measurements from the NOMAD experiment,” in: Proceedings of 32nd International Conference on High-Energy Physics (ICHEP’04), Beijing, China, August 16–22, 2004, ed. by H. Chen, D. Du, W. Li, C. Lu (Hackensack, World Scientific, 2005), Vol. **1**, p. 468 [arXiv:hep-ex/0411032]
 59. V. V. Lyubushkin, B. A. Popov, “A study of quasielastic neutrino interactions $\nu_{\mu} n \rightarrow \mu^- p$ in the NOMAD experiment,” *Yad. Fiz.* **69**, 1917 (2006) [*Phys. Atom. Nucl.* **69**, 1876 (2006)]
 60. A. Martinez de la Ossa Romero, “Study of accelerator neutrino interactions in a liquid argon TPC,” arXiv:hep-ex/0703026
 61. V. V. Lyubushkin, Ph.D. Thesis, JINR, Dubna, 2008 (in preparation)
 62. V. V. Makeev et al., “Quasielastic neutrino scattering $\nu_{\mu} n \rightarrow \mu^- p$ at 2 to 20 GeV in bubble chamber SKAT,” *Pisma Zh. Eksp. Teor. Fiz.* **34**, 418 (1981) [*JETP Lett.* **34**, 397 (1981)]
 63. S. V. Belikov et al. (IHEP-ITEP Collaboration), “Quasielastic neutrino and antineutrino interactions at the Serpukhov accelerator,” preprint IFVE 81-146 ONF SERP-E-45, Serpukhov, 1981 (unpublished)
 64. S. V. Belikov et al., “Neutrino and antineutrino quasielastic scattering at 3 to 30 GeV,” preprint IFVE 82-107 ONF SERP-E-45, Serpukhov, 1982 (unpublished)
 65. S. V. Belikov et al., “Quasielastic $\nu_{\mu} n$ scattering at energy 3–30 GeV,” *Yad. Fiz.* **35**, 59 (1982) [*Sov. J. Nucl. Phys.* **35**, 35 (1982)]
 66. S. V. Belikov et al., “Bounds on neutrino oscillation parameters from quasielastic scattering in the Serpukhov neutrino beams,” *Pisma Zh. Eksp. Teor. Fiz.* **38**, 547 (1983) [*JETP Lett.* **38**, 661 (1983)]
 67. S. V. Belikov et al., “Restrains on parameters of oscillations of muon neutrinos from quasielastic scattering data,” *Yad. Fiz.* **41**, 919 (1985) [*Sov. J. Nucl. Phys.* **41**, 589 (1985)]
 68. S. V. Belikov et al., “Quasielastic neutrino and antineutrino scattering: total cross-sections, axial-vector form-factor,” *Z. Phys. A* **320**, 625 (1985)

69. H. J. Grabosch et al. (SKAT Collaboration), preprints PHE 86-11, Berlin-Zeuthen, 1986 and IFVE 86-221 ONF SERP-E-107, Serpukhov, 1986 (unpublished)
70. H. J. Grabosch et al., “Study of the quasielastic reactions $\nu n \rightarrow \mu^- p$ and $\bar{\nu} p \rightarrow \mu^+ n$ in the SKAT bubble chamber at energies 3–20 GeV,” *Yad. Fiz.* **47**, 1630 (1988) [*Sov. J. Nucl. Phys.* **47**, 1032 (1988)]
71. J. Brunner et al. (SKAT Collaboration), “Quasielastic nucleon and hyperon production by neutrinos and antineutrinos with energies below 30 GeV,” *Z. Phys. C* **45**, 551 (1990)
72. A. Bodek, S. Avvakumov, R. Bradford, H. Budd, “Duality constrained parameterization of vector and axial nucleon form factors,” *Eur. Phys. J. C* **53**, 349 (2008) [arXiv:0708.1946 [hep-ex]]; see also A. Bodek, S. Avvakumov, R. Bradford, H. Budd, “Modeling atmospheric neutrino interactions: Duality constrained parameterization of vector and axial nucleon form factors,” arXiv:0708.1827 [hep-ex]
73. E. L. Lomon, “Effect of revised R_n measurements on extended Gari-Krümpelmann model fits to nucleon electromagnetic form factors,” arXiv:nucl-th/0609020
74. A. Strumia, F. Vissani, “Precise quasielastic neutrino/nucleon cross-section,” *Phys. Lett. B* **564**, 42 (2003) [arXiv:astro-ph/0302055]
75. K. S. Kuzmin, V. V. Lyubushkin, V. A. Naumov, “Tau lepton polarization in quasielastic neutrino-nucleon scattering,” *Nucl. Phys. B Proc. Suppl.* **139**, 154 (2005) [arXiv:hep-ph/0408107]
76. K. S. Kuzmin, V. V. Lyubushkin, V. A. Naumov, “Axial masses in quasielastic neutrino scattering and single-pion neutrino production on nucleons and nuclei,” *Acta Phys. Polon. B* **37**, 2337 (2006) [arXiv:hep-ph/0606184]
77. C. H. Llewellyn Smith, “Neutrino reactions at accelerator energies,” *Phys. Rept.* **3 C**, 261 (1972)
78. D. H. Wilkinson, “Limits to second-class nucleonic and mesonic currents,” *Eur. Phys. J. A* **7**, 307 (2000); D. H. Wilkinson, “Limits to second-class nucleonic currents,” *Nucl. Instrum. Meth. A* **456**, 655 (2000); D. H. Wilkinson, “Second-class currents and Δs in $\nu(\bar{\nu})p$ elastic scattering,” *ibid.*, **A 469**, 286 (2001)
79. S. Gardner, C. Zhang, “Sharpening low-energy, standard-model tests via correlation coefficients in neutron β decay,” *Phys. Rev. Lett.* **86**, 5666 (2001) [arXiv:hep-ph/0012098]
80. J. J. Kelly, “Simple parametrization of nucleon form factors,” *Phys. Rev. C* **70**, 068202 (2004)
81. M. F. Gari, W. Krümpelmann, “The electric neutron form-factor and the strange quark content of the nucleon,” *Phys. Lett. B* **274**, 159 (1992); *ibid.* **282**, 483 (E) (1992)
82. E. L. Lomon, “Extended Gari-Krümpelmann model fits to nucleon electromagnetic form factors,” *Phys. Rev. C* **64**, 035204 (2001) [arXiv:nucl-th/0104039]
83. E. L. Lomon, “Effect of recent R_p and R_n measurements on extended Gari-Krümpelmann model fits to nucleon electromagnetic form factors,” *Phys. Rev. C* **66**, 045501 (2002) [arXiv:nucl-th/0203081]
84. J. Arrington, “How well do we know the electromagnetic form factors of the proton?,” *Phys. Rev. C* **68**, 034325 (2003) [arXiv:nucl-ex/0305009]
85. J. Arrington, “How well do we know the electromagnetic form factors of the proton?,” *Eur. Phys. J. A* **17**, 311 (2003) [arXiv:hep-ph/0209243]
86. J. M. Finn (for the JLab E93-038 Collaboration), “Measurements of the electric form factor of the neutron at JLab via recoil polarimetry in the reaction: $d(e, e' n)p$,” *Fizika B* **13**, 545 (2004)
87. B. Anderson et al. (Jefferson Lab E95-001 Collaboration), “Extraction of the neutron magnetic form factor from quasi-elastic $^3\text{He}(e, e') Q^2 = 0.1 - 0.6 \text{ (GeV/c)}^2$,” *Phys. Rev. C* **75**, 034003 (2007) [arXiv:nucl-ex/0605006]
88. D. Day, “Nucleon elastic form factors: Current status of the experimental effort,” *Eur. Phys. J. A* **31**, 560 (2007)
89. C. F. Perdrisat, V. Punjabi, M. Vanderhaeghen, “Nucleon electromagnetic form factors,” *Prog. Part. Nucl. Phys.* **59**, 694 (2007) [arXiv:hep-ph/0612014]
90. K. Hagiwara, K. Mawatari, H. Yokoya, “Pseudoscalar form factors in tau-neutrino nucleon scattering,” *Phys. Lett. B* **591**, 113 (2004) [arXiv:hep-ph/0403076]
91. K. S. Kuzmin, V. V. Lyubushkin, V. A. Naumov, “Polarization of tau leptons produced in quasielastic neutrino nucleon scattering,” *Mod. Phys. Lett. A* **19**, 2919 (2004) [arXiv:hep-ph/0403110]
92. W. M. Yao et al. (Particle Data Group), “Review of particle physics,” *J. Phys. G* **33**, 1 (2006) and 2007 partial update for the 2008 edition, see URL <http://pdg.lbl.gov/>
93. D. Pocanic et al., “Precise measurement of the $\pi^+ \rightarrow \pi^0 e^+ \nu$ branching ratio,” *Phys. Rev. Lett.* **93**, 181803 (2004) [arXiv:hep-ex/0312030]
94. S. Nakamura et al. “Neutrino deuteron reactions at solar neutrino energies,” *Nucl. Phys. A* **707**, 561 (2002) [arXiv:nucl-th/0201062]
95. D. H. Perkins, “Neutrino interactions,” in: Proceedings of the 16th International Conference on High Energy Physics, National Accelerator Laboratory, Chicago-Batavia, Illinois, September 6–13, 1972, ed. by J. D. Jackson, A. Roberts (National Accelerator Laboratory, Batavia, Illinois, 1973), Vol. **IV**, p. 189
96. M. Derrick, “Charged current neutrino reactions in the resonance region,” in: Proceedings of the 17th International Conference on High Energy Physics, London, July 1–10, 1974, ed. by J. R. Smith (Rutherford High Energy Laboratory, Didcot, Berkshire, England, 1975), p. II-166
97. D. H. Perkins, “Review of neutrino experiments,” in: Proceedings of the 1975 International Symposium on Lepton and Photon Interactions at High Energies, Stanford University, August 21–27, 1975, ed. by T. W. Kirk (Stanford Linear Accelerator Center, Stanford, 1975), p. 571
98. D. Cline, W. F. Fry, “Neutrino scattering and new particle production,” *Ann. Rev. Nucl. Part. Sci.* **27**, 209 (1977)
99. H. Wachsmuth, “Accelerator neutrino physics,” Lectures held at the Herbstschule für Hochenergiephysik, Maria Laach, Eifel, Germany, September 14–24, 1976, preprint CERN/EP/PHYS 77-40, August 17, 1977 (unpublished)
100. P. F. Ermolov, A. I. Mukhin, “Neutrino experiments at high energies,” *Usp. Fiz. Nauk* **124**, 385 (1978) [*Sov. Phys. Uspekhi* **21**, 185-214 (1978)]
101. P. Musset, J.-P. Vialle, “Neutrino physics with Gargamelle,” *Phys. Rept.* **39**, 1 (1978)
102. S. I. Alekhin et al., “Compilation of cross-sections IV: $\gamma, \nu, A, \Sigma, \Xi, \Lambda$, and K_L^0 induced reactions,” Report CERN-HERA 87-01, European Organization for Nuclear Research, Geneva, 1987

103. M. Sakuda, “Results from low-energy neutrino nucleus scattering experiments,” Nucl. Phys. B Proc. Suppl. **112**, 109 (2002)
104. V. V. Ammosov et al., “Investigation of neutrino interactions using the bubble chamber SKAT,” Fiz. Elem. Chast. Atom. Yadra **23**, 648 (1992) [Sov. J. Part. Nucl. **23**, 283 (1992)]
105. C. Baltay, “Deep inelastic neutrino interactions and charm production,” Nucl. Phys. B Proc. Suppl. **36**, 363 (1994)
106. G. P. Zeller, “Low energy neutrino cross sections: Comparison of various Monte Carlo predictions to experimental data,” a talk at the 2nd International Workshop on Neutrino-Nucleus Interactions in the few-GeV Region, NuInt’02, University of California, Irvine, December 12–15, 2002; arXiv:hep-ex/0312061
107. B. Fleming, “Neutrino cross sections and scattering physics,” AIP Conf. Proc. **815**, 1 (2006)
108. M. Sorel, “Overview of progress in neutrino scattering measurements,” AIP Conf. Proc. **967**, 17 (2007) [arXiv:0710.3966 [hep-ex]]
109. R. Gran, “Progress in measuring neutrino quasielastic interactions,” AIP Conf. Proc. **967**, 141 (2007) [arXiv:0711.3024 [hep-ex]]
110. F. James, “MINUIT, Reference Manual, Version 94.1,” CERN Program Library Long Writeup D506 (European Organization for Nuclear Research, Geneva, 1994); F. James, M. Roos, “MINUIT: A system for function minimization and analysis of the parameter errors and correlations,” Comput. Phys. Commun. **10**, 343 (1975)
111. I. Budagov et al., “Single pion production by neutrinos on free protons,” Phys. Lett. **29B**, 524 (1969)
112. D. Allasia et al. (Amsterdam-Bergen-Bologna-Padova-Pisa-Saclay-Torino Collaboration), “Measurement of the ν_μ and $\bar{\nu}_\mu$ nucleon charged-current total cross sections, and the ratio of ν_μ neutron to ν_μ proton charged-current total cross sections,” Nucl. Phys. B **239**, 301 (1984)
113. S. K. Singh, “The effect of final state interactions and deuteron binding in $\nu d \rightarrow \mu^- pp$,” Nucl. Phys. B **36**, 419 (1972)
114. N. J. Baker et al., “Exclusive neutral-current reaction $\nu_\mu n \rightarrow \nu_\mu p \pi^-$ in the BNL 7-foot deuterium bubble chamber,” Phys. Rev. D **28**, 2900 (1983)
115. A. V. Butkevich, S. P. Mikheyev, “Test of Fermi gas model and plane-wave impulse approximation against electron nucleus scattering data,” Phys. Rev. C **72**, 025501 (2005) [arXiv:hep-ph/0505008]
116. A. V. Butkevich, S. A. Kulagin, “Quasi-elastic neutrino charged-current scattering cross sections on oxygen,” Phys. Rev. C **76**, 045502 (2007) [arXiv:0705.1051 [nucl-th]]; see also A. V. Butkevich, S. A. Kulagin, “QE neutrino CC cross sections off ^{16}O ,” AIP Conf. Proc. **967**, 298 (2007) [arXiv:0711.3223 [nucl-th]]
117. K. S. Kuzmin, V. V. Lyubushkin, V. A. Naumov, “Fine-tuning parameters to describe the total charged-current neutrino-nucleon cross section,” Yad. Fiz. **69**, 1898 (2006) [Phys. Atom. Nucl. **69**, 1857 (2006)]; K. S. Kuzmin, V. V. Lyubushkin, V. A. Naumov, “How to sum contributions into the total charged-current neutrino-nucleon cross section,” arXiv:hep-ph/0511308
118. M. H. Ahn et al. (K2K Collaboration), “Search for electron neutrino appearance in a 250 km long baseline experiment,” Phys. Rev. Lett. **93**, 051801 (2004) [arXiv:hep-ex/0402017]

119. M. H. Ahn et al. (K2K Collaboration), “Measurement of neutrino oscillation by the K2K experiment,” Phys. Rev. D **74**, 072003 (2006) [arXiv:hep-ex/0606032]
120. Y. Ashie et al. (Super-Kamiokande Collaboration), “A measurement of atmospheric neutrino oscillation parameters by Super-Kamiokande I,” Phys. Rev. D **71**, 112005 (2005) [arXiv:hep-ex/0501064]

ADDITIONAL REFERENCES

121. X. Espinal, F. Sánchez, “Measurement of the axial vector mass in neutrino-Carbon interactions at K2K,” AIP Conf. Proc. **967**, 117 (2007)
122. H. Budd, A. Bodek, J. Arrington, “Vector and axial form factors applied to neutrino quasielastic scattering,” Nucl. Phys. B Proc. Suppl. **139**, 90 (2005) [arXiv:hep-ex/0410055]

Note on the recent SciBar result

In the recent paper by Espinal and Sánchez [121],⁶ the nucleon axial-vector form factor has been determined from an analysis of neutrino-Carbon interactions in the K2K detector fully active SciBar tracking calorimeter. The best fit value of the axial-vector mass obtained in this analysis from the Q^2 distribution of events and using the BBA(04) vector form factors [122] is

$$M_A^{(\text{SciBar})} = 1.144 \pm 0.077 \text{ (fit)}_{-0.072}^{+0.078} \text{ (syst) GeV}$$

(with $\chi^2/\text{NDF} = 17.2/9$, $8/9$, and $9.8/9$ for, respectively, 1-track, 2-track QE, and 2-track non-QE events). It is in agreement with M_A previously measured at SciFi detector in K2K [4]. Formally (within the quoted errors) the SciBar result does not contradict to the world average value (12) but does not support it.

⁶ Which became available to us when this paper has already been published

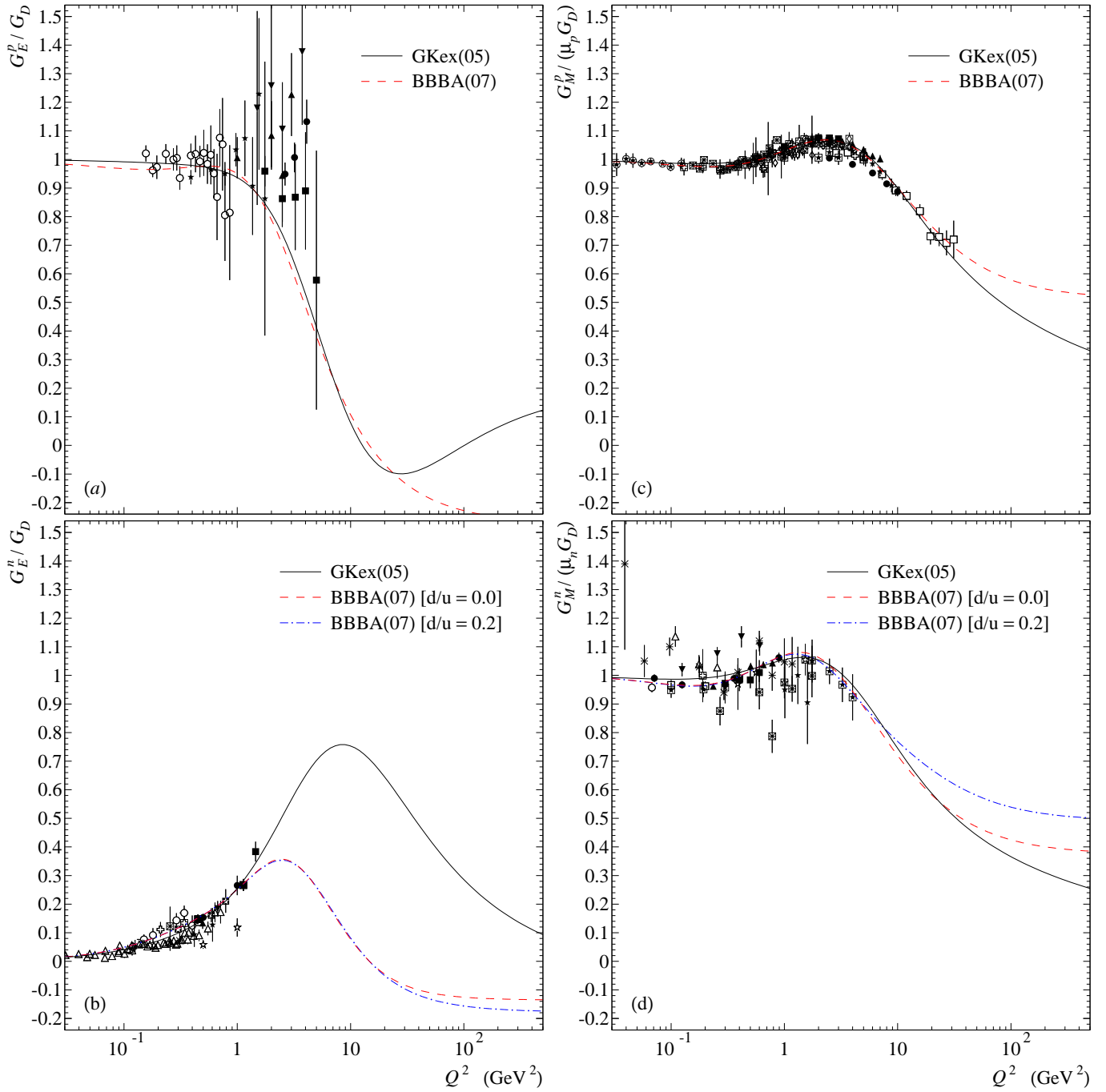


Fig. 1. Comparison of the GKex(05) and BBBA(07) models for the electric and magnetic form factors of proton and neutron (divided by the standard dipole G_D) with the data from electron scattering experiments. The data compilation is taken from Refs. [84, 85, 86, 87, 88, 89]. The two versions of the BBBA(07) parametrization are shown for the neutron form factors.

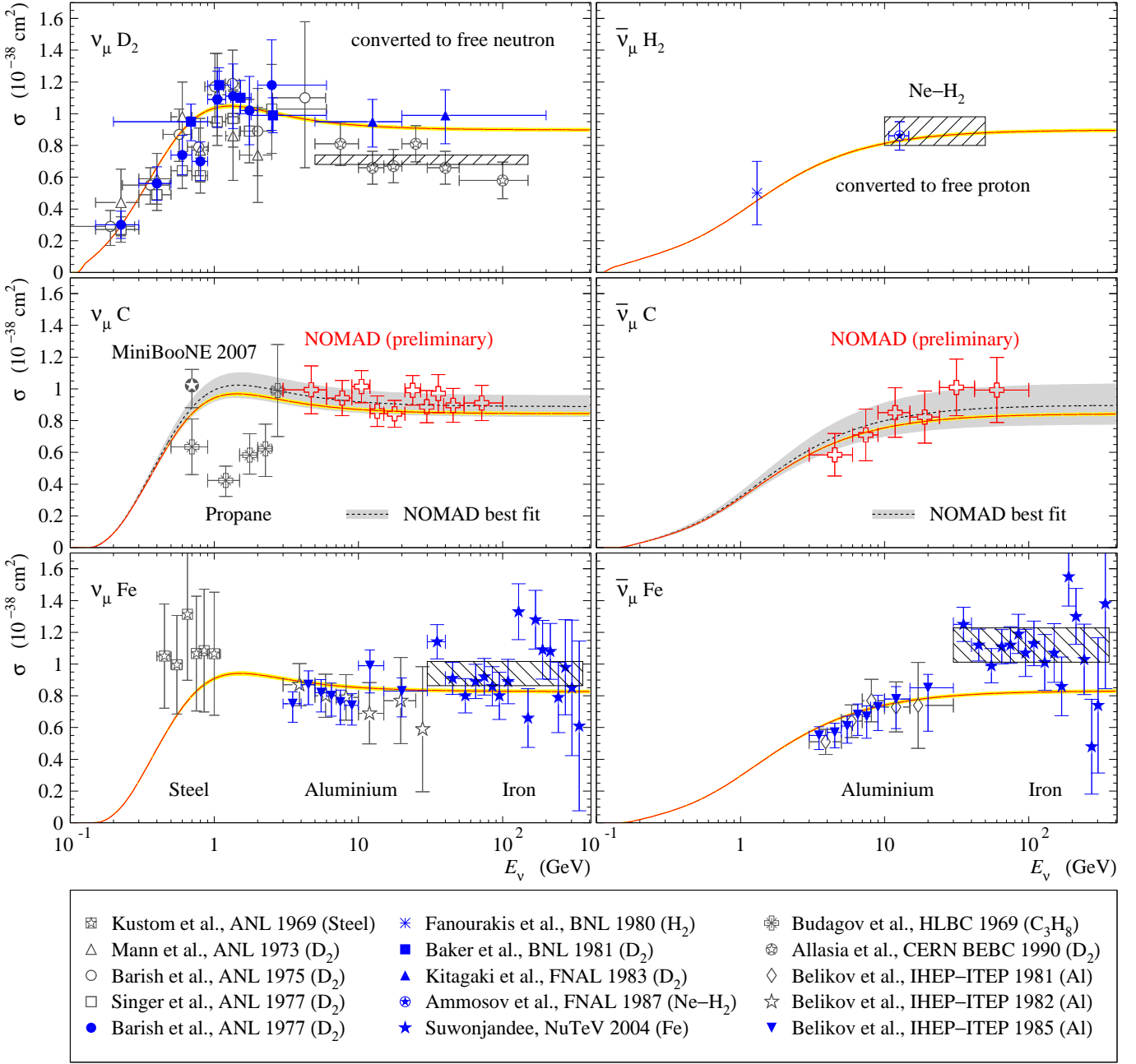


Fig. 2. Total quasielastic $\nu_\mu n$ and $\bar{\nu}_\mu p$ cross sections measured in experiments with deuterium, hydrogen, carbon/propane, aluminium, and iron/steel targets at ANL 1969 [12], ANL 1973 [14], ANL 1975 [15], ANL 1977 [16,17], BNL 1980 [21], BNL 1981 [22], FNAL 1983 [32], FNAL E180 1984 [33,34] (rectangle in top right panel), FNAL E180 1987 [36], NuTeV 2004 [37] (points and rectangles in bottom panels), CERN HLBC 1969 [43], CERN BEBC 1990 [57] (points and rectangle in top left panel), CERN NOMAD 2008 [61] (preliminary), IHEP-ITEP 1981 [63], IHEP-ITEP 1982 [65], and IHEP-ITEP 1985 [67,68]. The deuterium and neon-hydrogen data were converted to a free neutron/proton target by the authors of the experiments. The MiniBooNE 2007 point [5] recalculated from the reported value of $M_A = 1.23 \pm 0.20$ GeV is also shown for comparison. The error bars represent the total errors which include the flux normalization uncertainties. The solid curves and narrow shaded bands are calculated with the BBBA(07) model for the vector form factors, with $M_A = 0.999 \pm 0.011$ GeV, the value obtained from the global fit to a subset of the full data set of total and differential cross sections (233 data points). The points shown by grey symbols are excluded from the fit, being either superseded by newer experiments, or not satisfying our selection criteria. The dashed curves and corresponding bands are the cross sections obtained by fitting the NOMAD 2008 alone with the GKex(2005) vector form factors (separately for ν_μ and $\bar{\nu}_\mu$ data).

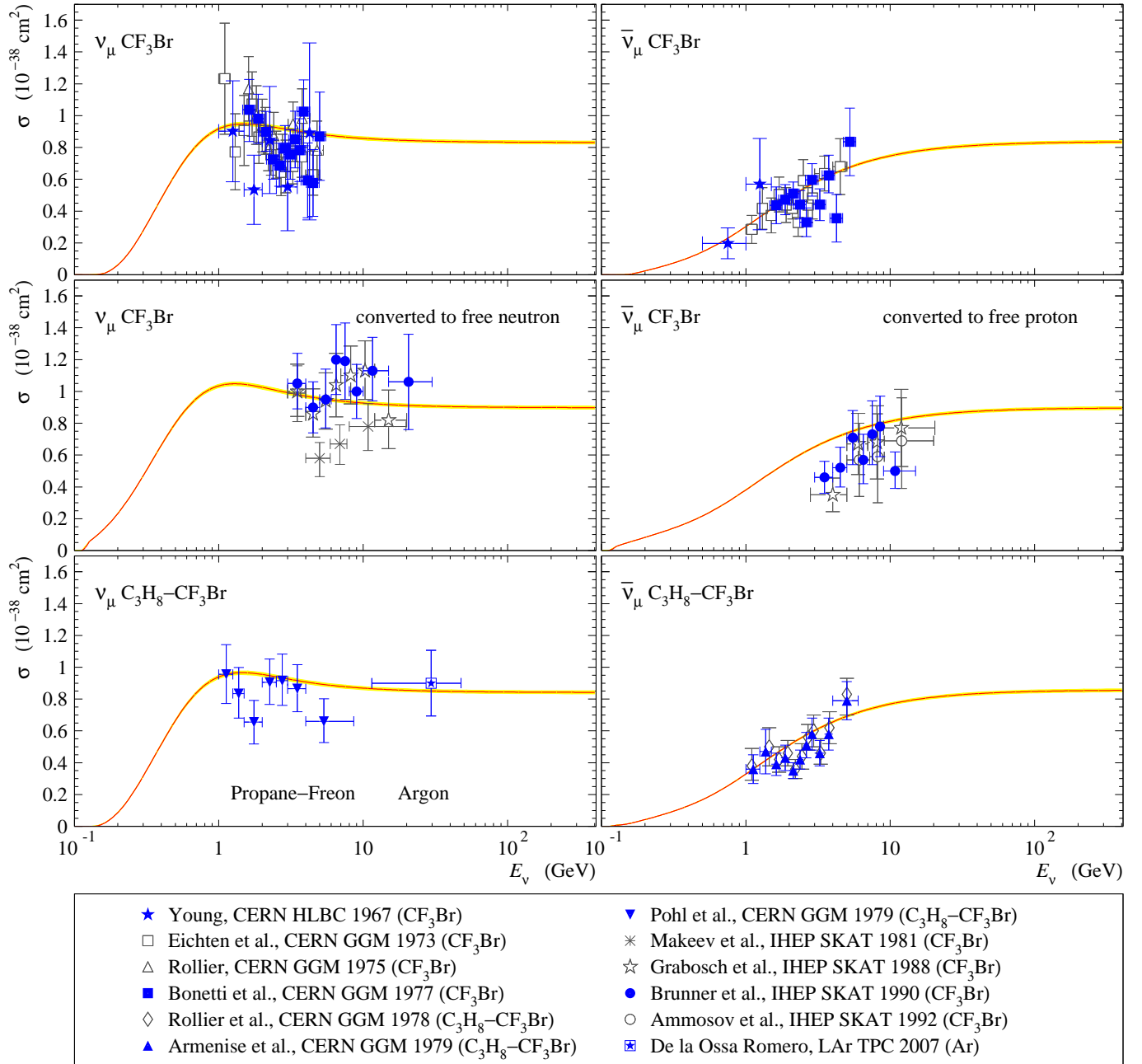


Fig. 3. Total quasielastic $\nu_\mu n$ and $\bar{\nu}_\mu p$ cross sections measured with the freon and propane-freon filled bubble chamber experiments CERN HLBC 1966 [39], CERN HLBC 1967 [40], CERN GGM 1973 [45], CERN GGM 1975 [48,97], CERN GGM 1977 [50], CERN GGM 1978 [52], CERN GGM 1979 [56,55], IHEP SKAT 1981 [62], IHEP SKAT 1988 [70], IHEP SKAT 1990 [71], and IHEP SKAT 1992 [104]. The point recently obtained in experiment with the Liquid Argon Time Projection Chamber (LAr TPC 2007) [60] is also shown. The SKAT datapoints were converted from freon to a free neutron/proton target by the authors of the experiments. The error bars represent the total errors which include the uncertainties due to flux normalization and nuclear Monte Carlo. The solid curves and narrow shaded bands are calculated with the BBBA(07) model for the vector form factors, with the global fit value of $M_A = 0.999 \pm 0.011 \text{ GeV}$. See caption of Fig. 2 for more details.

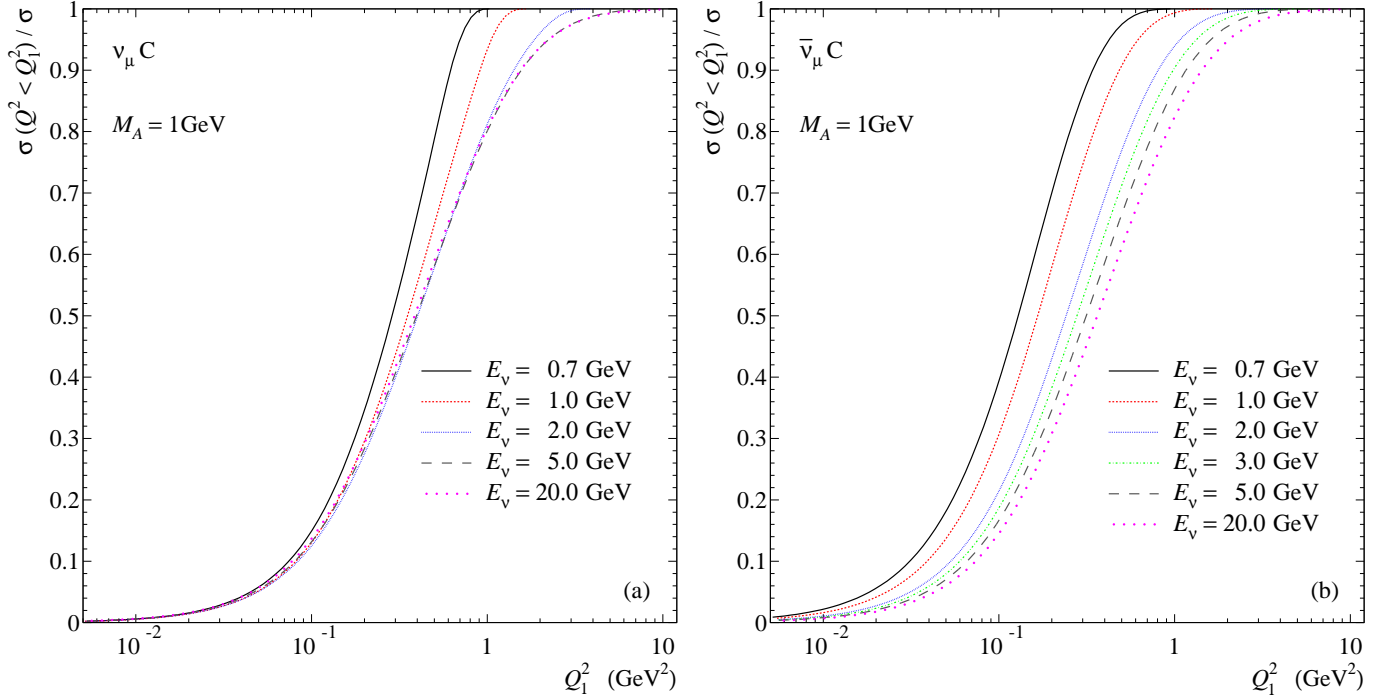


Fig. 4. The ratio $R = \sigma(Q^2 < Q_1^2) / \sigma$ vs. Q_1^2 , evaluated for ν_μ and $\bar{\nu}_\mu$ quasielastic interactions with carbon target at several (anti)neutrino energies. The M_A value is taken to be 1 GeV.

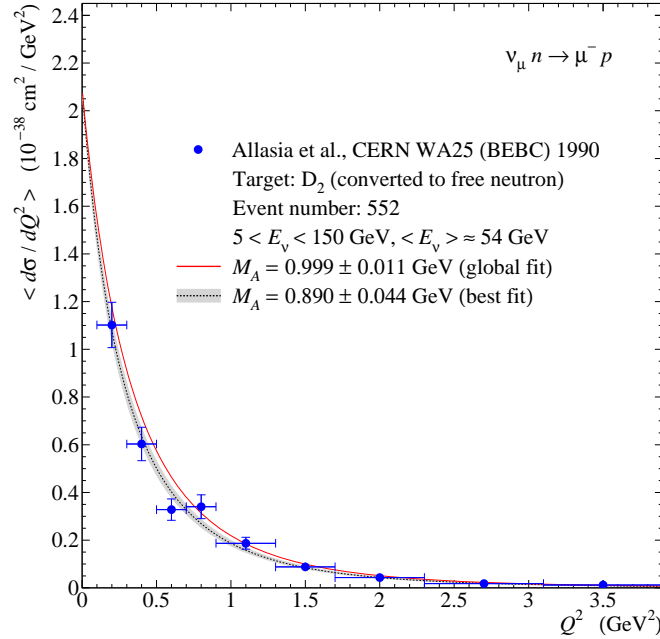


Fig. 5. Flux-weighted differential cross section for $\nu_\mu n \rightarrow \mu^- p$ measured in the WA25 experiment with the CERN bubble chamber BEBC filled with deuterium and exposed to high-energy ν_μ beam at the CERN-SPS [57]. The data were converted to a free neutron target by the authors of the experiment. The curves are the calculated cross sections averaged over the experimental ν_μ energy spectrum borrowed from Ref. [112]. The energy range and estimated mean energy are given in the legend. The dashed curves are for the best fit to the WA25 data, while the solid curves correspond to the global fit to all QES data. Shaded band represents 1σ deviation from the best-fitted value of M_A given in the legend.

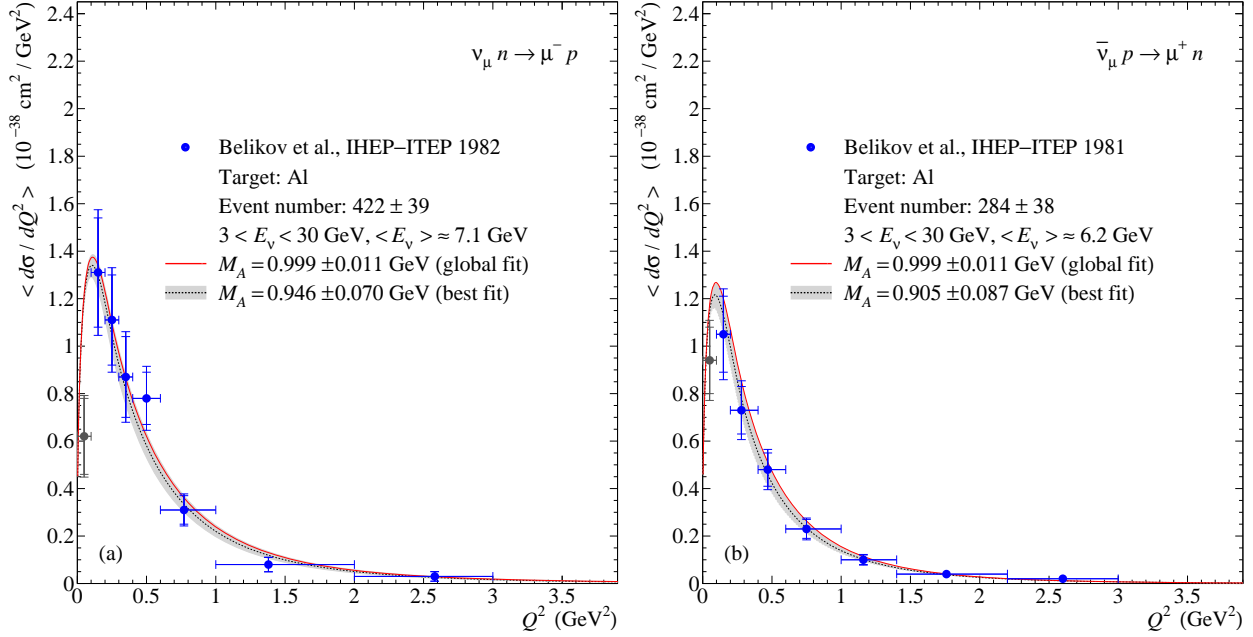


Fig. 6. Flux-weighted differential cross sections for $\nu_\mu n \rightarrow \mu^- p$ (a) and $\bar{\nu}_\mu p \rightarrow \mu^+ n$ (b) measured in the IHEP-ITEP experiment with a spark chamber detector with aluminium filters and exposed to the U70 broad-band ν_μ and $\bar{\nu}_\mu$ beams of the Serpukhov PS [63,65]. The inner and outer bars indicate statistical and total errors, respectively; the overall systematic error of about 10% is due mainly to uncertainties of the flux normalization and scanning/triggering efficiencies. The curves are the calculated cross sections averaged over the experimental ν_μ and $\bar{\nu}_\mu$ energy spectra borrowed from Refs. [68,104]. The energy range and estimated mean energies are given in the legends. The dashed curves are for the best fit to the IHEP-ITEP data, while the solid curves correspond to the global fit to all QES data. The points shown by grey symbols are excluded from the fits (see text). Shaded bands represent 1σ deviations from the best-fitted values of M_A given in the legends.

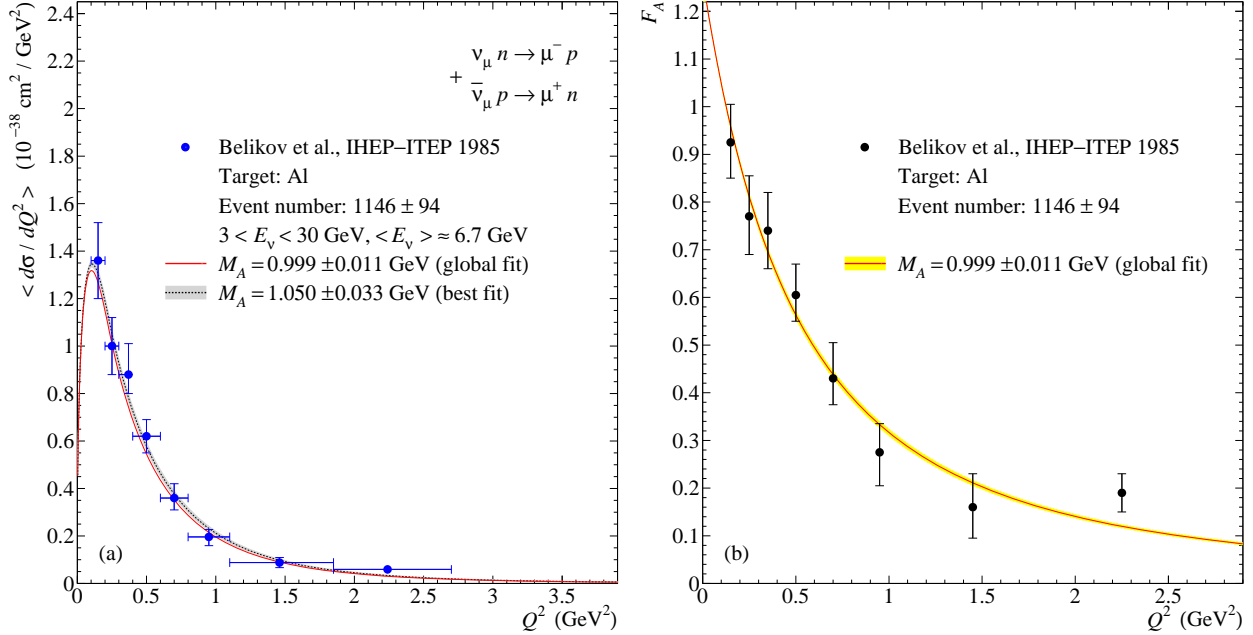


Fig. 7. Flux-weighted semisum of differential cross sections for $\nu_\mu n \rightarrow \mu^- p$ and $\bar{\nu}_\mu p \rightarrow \mu^+ n$ (a) and axial-vector form factor $F_A(Q^2)$ (b) measured in the IHEP-ITEP experiment with a spark chamber detector with aluminium filters and exposed to the U70 broad-band ν_μ and $\bar{\nu}_\mu$ beams of the Serpukhov PS [68]. The error bars represent the total errors which include the overall systematic error of about 10% (due mainly to uncertainties of the flux normalization and scanning/triggering efficiencies). The curves in panel (a) are the calculated semisum of the cross sections each averaged over the experimental ν_μ and $\bar{\nu}_\mu$ energy spectra borrowed from Refs. [68,104]. The energy range and estimated mean energy are given in the legend. The dashed curve is for the best fit to the quoted IHEP-ITEP data, while the solid curve corresponds to the global fit to all QES data. Shaded bands in panels (a) and (b) represent 1σ deviations from the best-fitted values of M_A given in the legends.

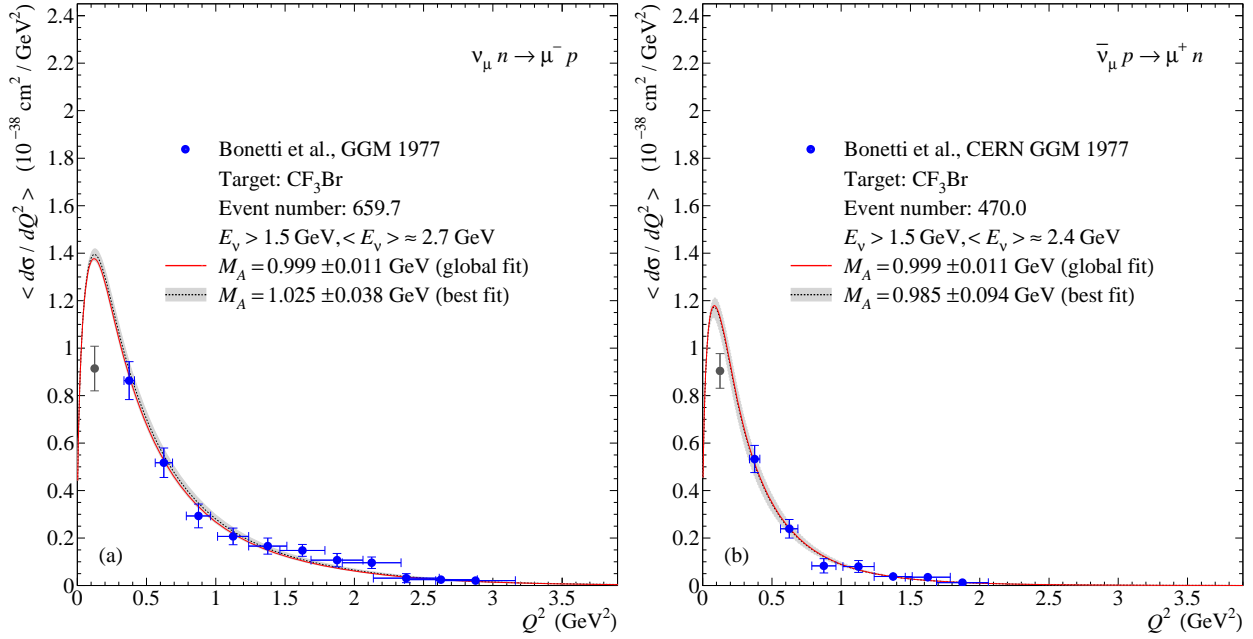


Fig. 8. Flux-weighted differential cross sections for $\nu_\mu n \rightarrow \mu^- p$ (a) and $\bar{\nu}_\mu p \rightarrow \mu^+ n$ (b) measured with the heavy-liquid bubble chamber Gargamelle filled with heavy freon and exposed to the CERN-PS ν_μ and $\bar{\nu}_\mu$ beams [50, 101]. The error bars contain the statistical fluctuation and the indetermination on the ν_μ and $\bar{\nu}_\mu$ fluxes. The curves are the calculated cross sections averaged over the experimental ν_μ and $\bar{\nu}_\mu$ energy spectra given in Ref. [50]. Only the events with $E_{\nu, \bar{\nu}} > 1.5 \text{ GeV}$ were accepted. The dashed curves are for the best fit to the GGM 1977 data, while the solid curves correspond to the global fit to all QES data. The points shown by grey symbols are excluded from the fits (see text). Shaded bands represent 1σ deviations from the best-fitted values of M_A given in the legends.

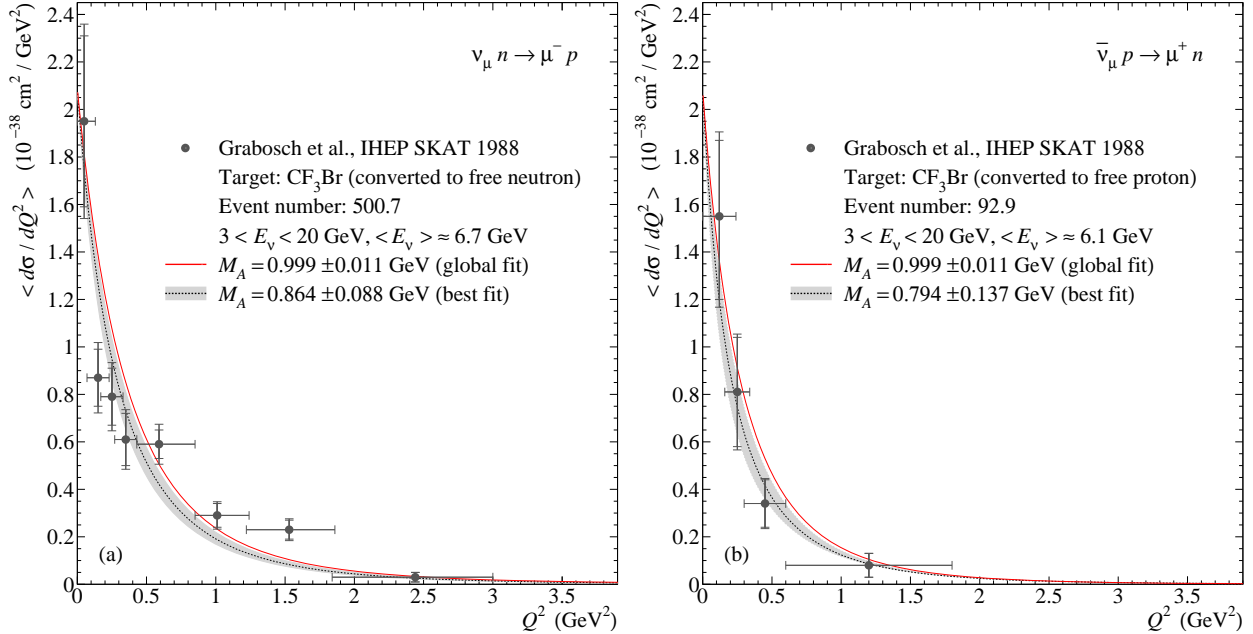


Fig. 9. Flux-weighted differential cross sections for $\nu_\mu n \rightarrow \mu^- p$ (a) and $\bar{\nu}_\mu p \rightarrow \mu^+ n$ (b) measured with the freon filled bubble chamber SKAT exposed to the U70 broad-band ν_μ and $\bar{\nu}_\mu$ beams of the Serpukhov PS [70, 104] (see also Refs. [69] for the earlier analyses of the same data sample). The data were converted to a free nucleon target by the authors of the experiment. The inner and outer bars indicate statistical and total errors, respectively; the systematic error includes the uncertainties due to the cross section normalization and nuclear Monte Carlo. The curves are the calculated cross sections averaged over the experimental ν_μ and $\bar{\nu}_\mu$ energy spectra borrowed from Ref. [104]. The energy range and estimated mean energies are given in the legends. The dashed curves are for the best fit to the SKAT 1988 data, while the solid curves correspond to the global fit to all QES data (the SKAT 1988 data are excluded from the global fit). Shaded bands represent 1σ deviations from the best-fitted values of M_A given in the legends.

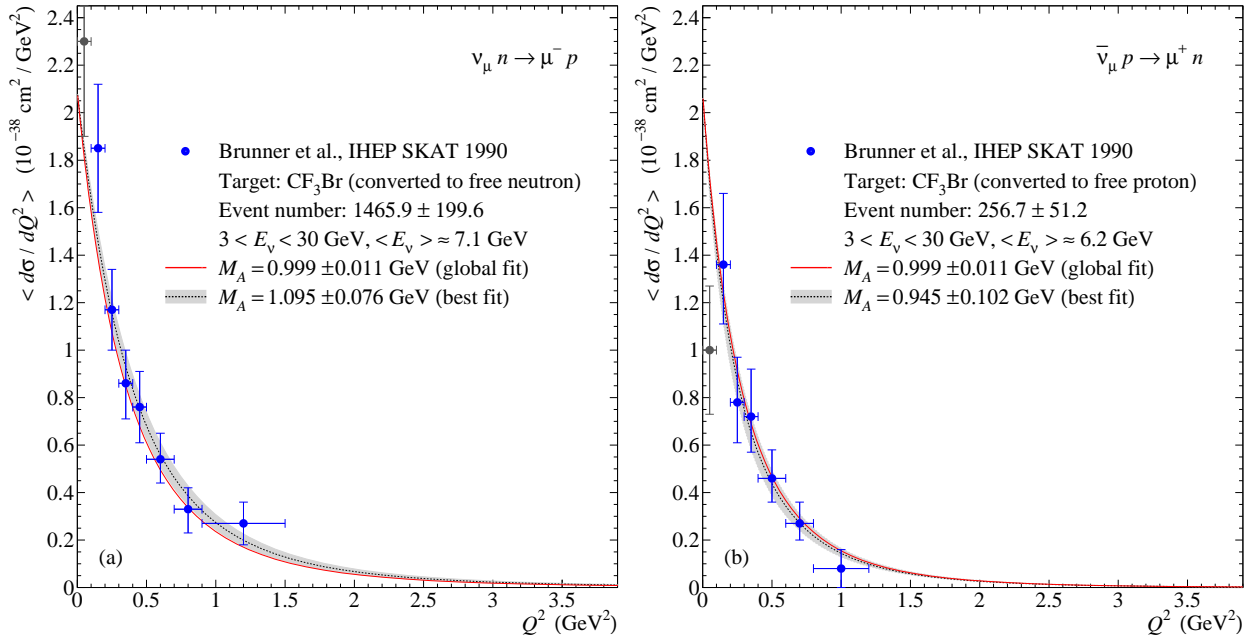


Fig. 10. Flux-weighted differential cross sections for $\nu_\mu n \rightarrow \mu^- p$ (a) and $\bar{\nu}_\mu p \rightarrow \mu^+ n$ (b) measured with the freon filled bubble chamber SKAT exposed to the U70 broad-band ν_μ and $\bar{\nu}_\mu$ beams of the Serpukhov PS [71]. The data were converted to a free nucleon target by the authors of the experiment. The inner and outer bars indicate statistical and total errors, respectively; the systematic error includes the uncertainties due to the cross section normalization and nuclear Monte Carlo. The curves are the calculated cross sections averaged over the experimental ν_μ and $\bar{\nu}_\mu$ energy spectra borrowed from Ref. [104]. The energy range and estimated mean energies are given in the legends. The dashed curves are for the best fit to the SKAT 1990 data, while the solid curves correspond to the global fit to all QES data. The points shown by grey symbols are excluded from the fits (see text). Shaded bands represent 1σ deviations from the best-fitted values of M_A given in the legends.

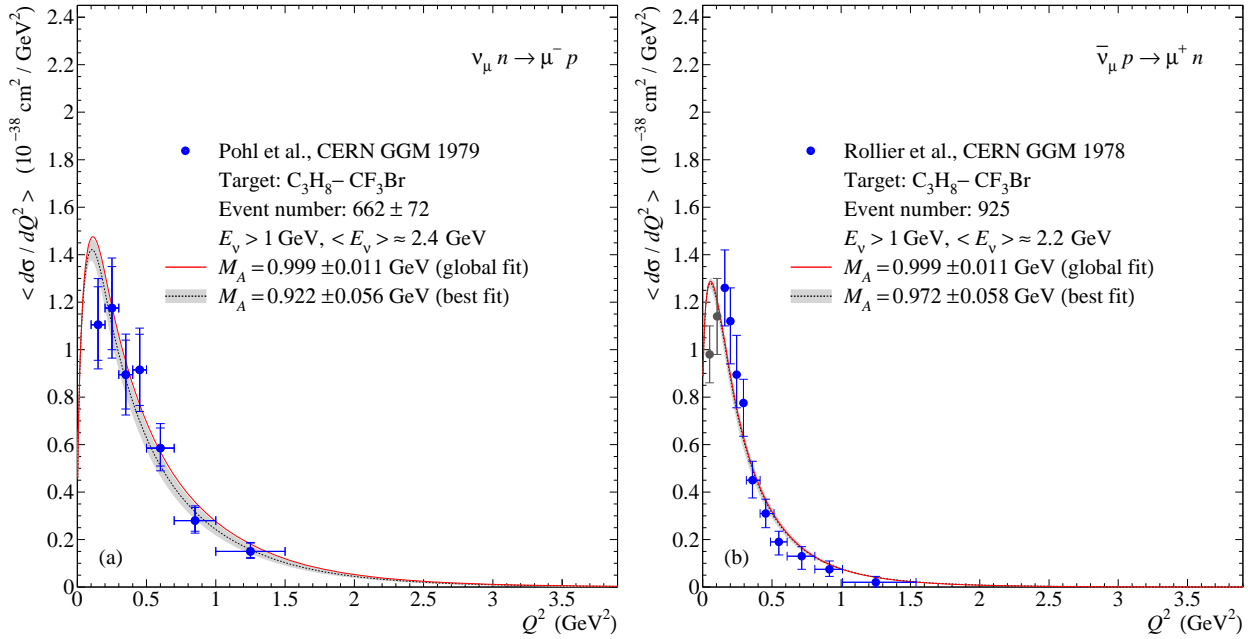


Fig. 11. Flux-weighted differential cross sections for $\nu_\mu n \rightarrow \mu^- p$ (a) and $\bar{\nu}_\mu p \rightarrow \mu^+ n$ (b) measured with the bubble chamber Gargamelle filled with light propane–freon mixture and exposed to the CERN-PS ν_μ and $\bar{\nu}_\mu$ beams [55, 52]. The inner and outer bars in panel (a) indicate statistical and total errors, respectively; the error bars in panel (b) contain the statistical fluctuation and the indetermination on the $\bar{\nu}_\mu$ flux. The curves are the calculated cross sections averaged over the experimental ν_μ and $\bar{\nu}_\mu$ energy spectra given in Refs. [50] and [56], respectively. Only the events with $E_{\nu, \bar{\nu}} > 1 \text{ GeV}$ were accepted. The dashed curves are for the best fit to the GGM data, while the solid curves correspond to the global fit to all QES data. The points shown by grey symbols are excluded from the fits (see text). Shaded bands represent 1σ deviations from the best-fitted values of M_A given in the legends.

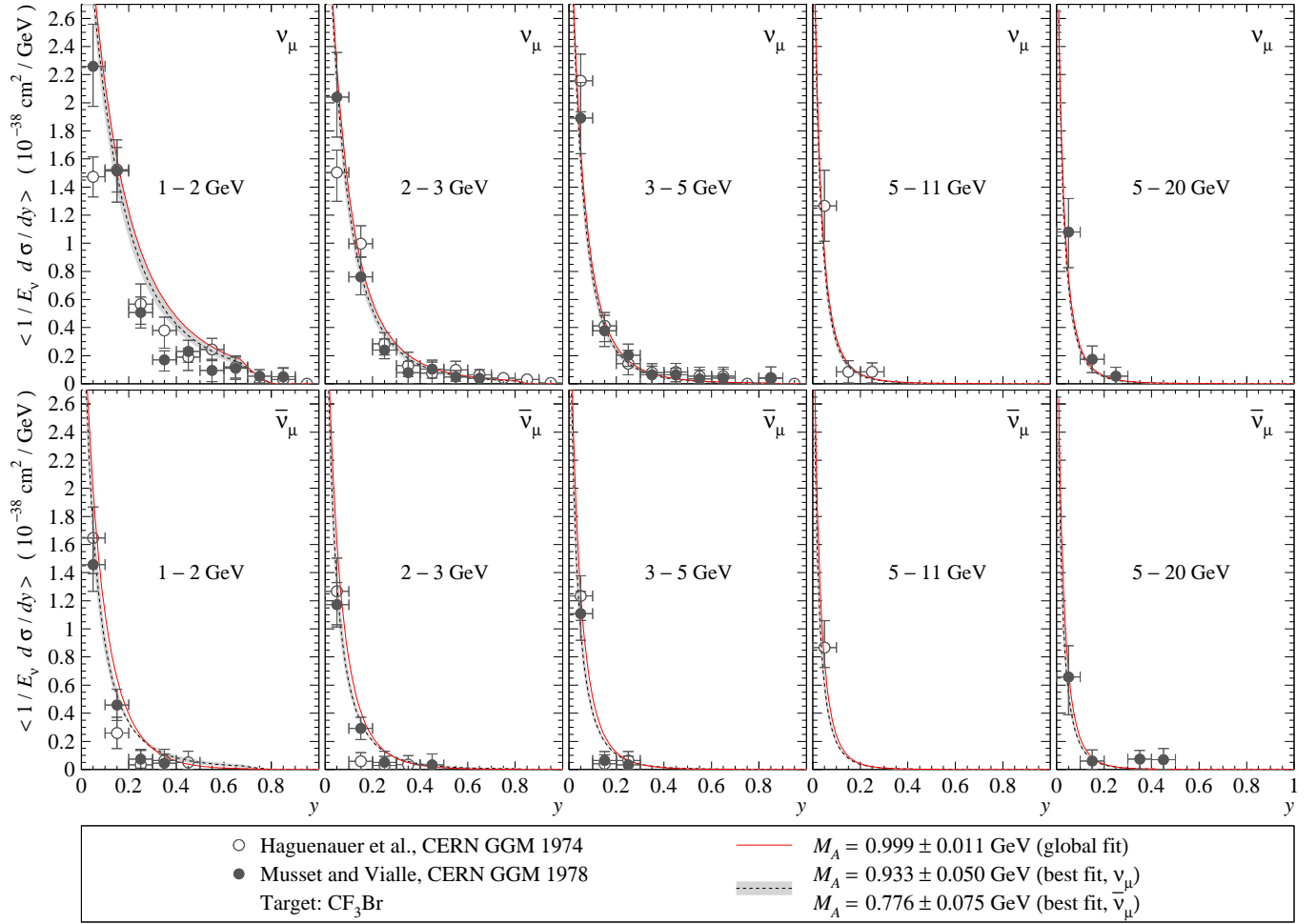


Fig. 12. Flux-weighted differential cross sections $(1/E_\nu)d\sigma(\nu_\mu n \rightarrow \mu^- p)/dy$ (top panels) and $(1/E_\nu)d\sigma(\bar{\nu}_\mu p \rightarrow \mu^+ n)/dy$ (bottom panels) measured with the heavy freon filled bubble chamber Gargamelle exposed to the wide-band CERN-PS ν_μ and $\bar{\nu}_\mu$ beams [47,101]. The data from Refs. [47] (range 5–11 GeV) and [101] (ranges 1–2, 2–3, 3–5, and 5–20 GeV) represent two different analyses of the same data sample (see also Refs. [46,49,105] for other versions). The measured cross sections were converted to a free nucleon target by the authors of the experiment. The quoted error bars are the total errors which include the uncertainties in the ν_μ and $\bar{\nu}_\mu$ fluxes and nuclear Monte Carlo. The curves are for the calculated cross sections averaged (for each energy range indicated in the panels) over the experimental ν_μ and $\bar{\nu}_\mu$ energy spectra taken from Ref. [101]. The dashed curves correspond to the M_A values obtained by fitting the GGM 1978 data from the energy ranges 2–3, 3–5, and 5–20 GeV and GGM 1974 data from the range 5–11 GeV (separately for neutrino and antineutrino cross sections). The range 1–2 GeV is excluded from the analysis in order to minimize the error in modelling the nuclear effects. The solid curves correspond to the global fit to all QES data (the GGM data are not included in this fit). Shaded bands represent 1σ deviations from the best-fitted values of M_A given in the legend.

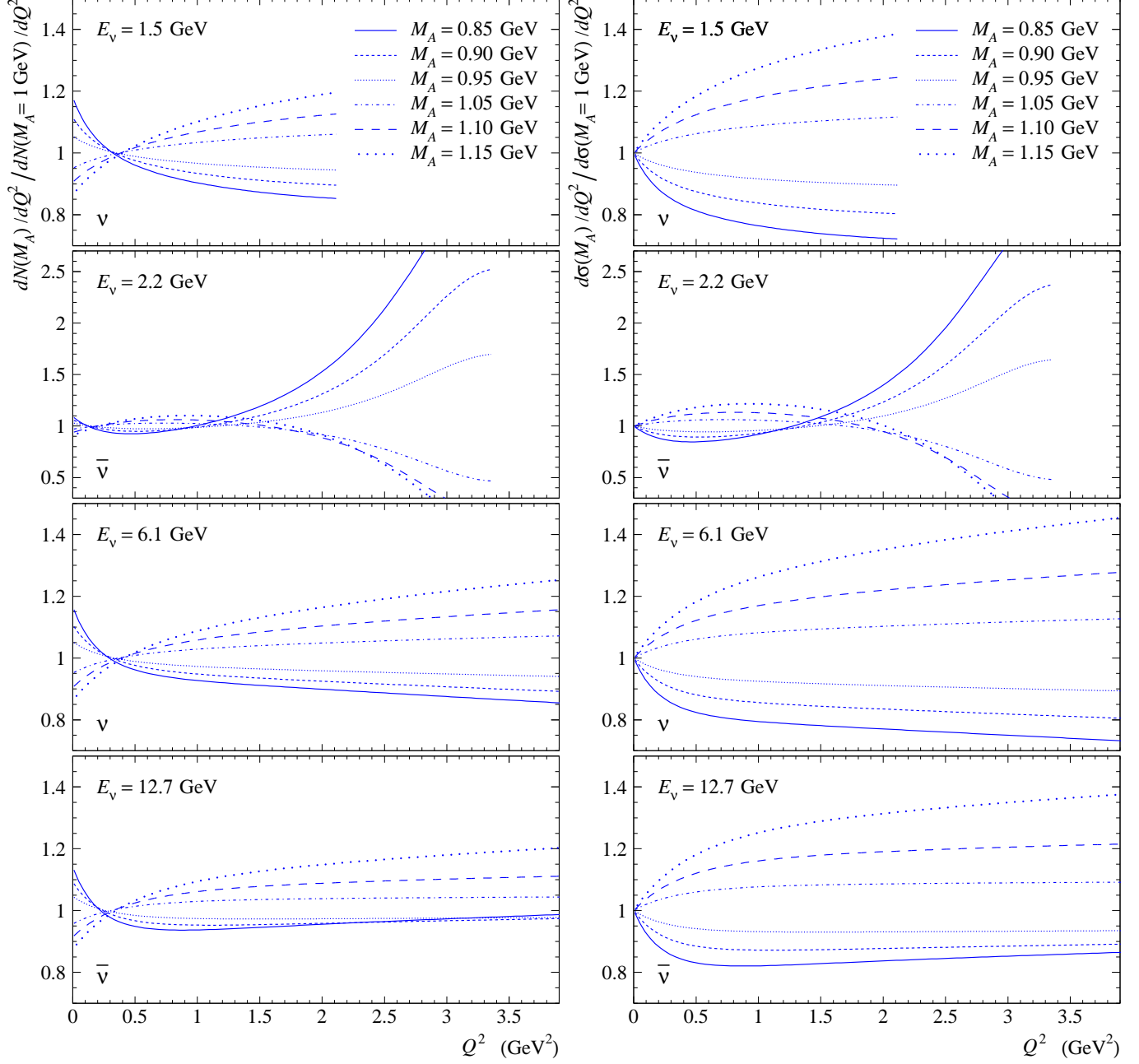


Fig. 13. The distributions dN/dQ^2 and differential cross sections $d\sigma/dQ^2$ vs. Q^2 for $\nu_\mu n$ and $\bar{\nu}_\mu p$ quasielastic scattering, calculated with different $M_A = 0.85, 0.90, 0.95, 1.05, 1.10$, and 1.15 GeV and normalized to the corresponding quantities calculated with $M_A = 1$ GeV at four fixed values of energy corresponding to the mean (anti)neutrino beam energies in experiments HLBC 1969 [43], Gargamelle 1979 [56], SKAT 1981 [62], and FNAL 1984 [33,34] (see Figs. 14–17 below). The curves in the four upper panels end up at the kinematical boundaries.

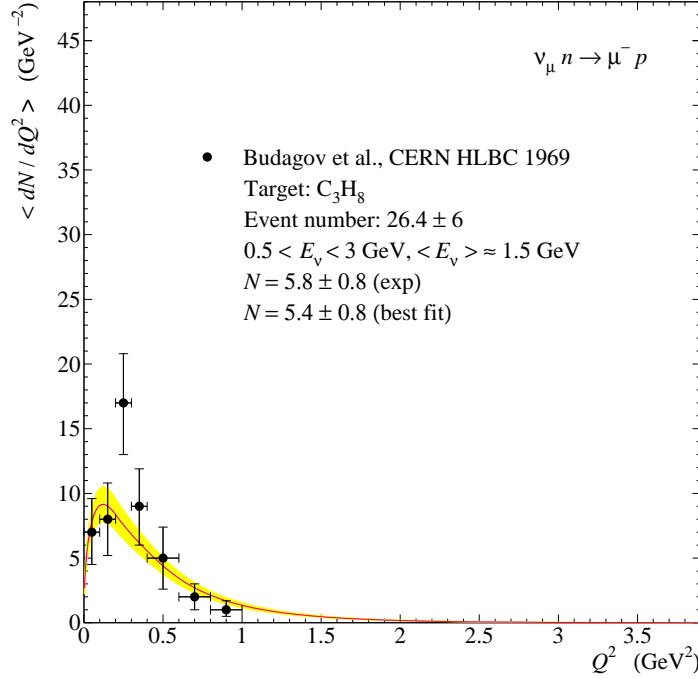


Fig. 14. Flux-weighted Q^2 distribution for $\nu_\mu n \rightarrow \mu^- p$ measured with the CERN heavy-liquid bubble chamber (HLBC) filled with propane and exposed to the CERN PS ν_μ beam [43]. The curve is the distribution calculated with M_A obtained from the global fit, averaged over the experimental ν_μ energy spectrum from Ref. [111], and normalized to the HLBC 1969 data. The spectrum is estimated to be accurate within $\pm 15\%$ (the error includes an estimate of systematic effects). The energy range and estimated mean energy are given in the legends. Shaded band represents 1σ variation from the average due to uncertainties in M_A and normalization factor N .

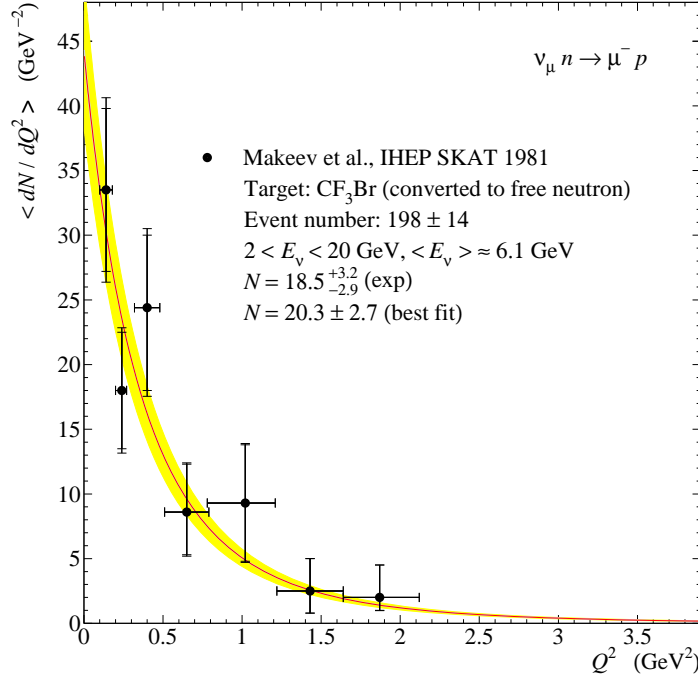


Fig. 15. Flux-weighted Q^2 distribution for $\nu_\mu n \rightarrow \mu^- p$ measured with the freon filled bubble chamber SKAT exposed to the U70 broad-band ν_μ beam of the Serpukhov PS [62]. The data were converted to a free nucleon target by the authors of the experiment. The inner and outer bars indicate statistical and total errors, respectively; the systematic error includes the uncertainties due to the flux normalization and nuclear Monte Carlo. The curve is the distribution calculated with M_A obtained from the global fit, averaged over the experimental ν_μ energy spectrum from Ref. [104], and normalized to the SKAT 1981 data. The energy range and estimated mean energy are given in the legends. Shaded band represents 1σ variation from the average due to uncertainties in M_A and normalization factor N .

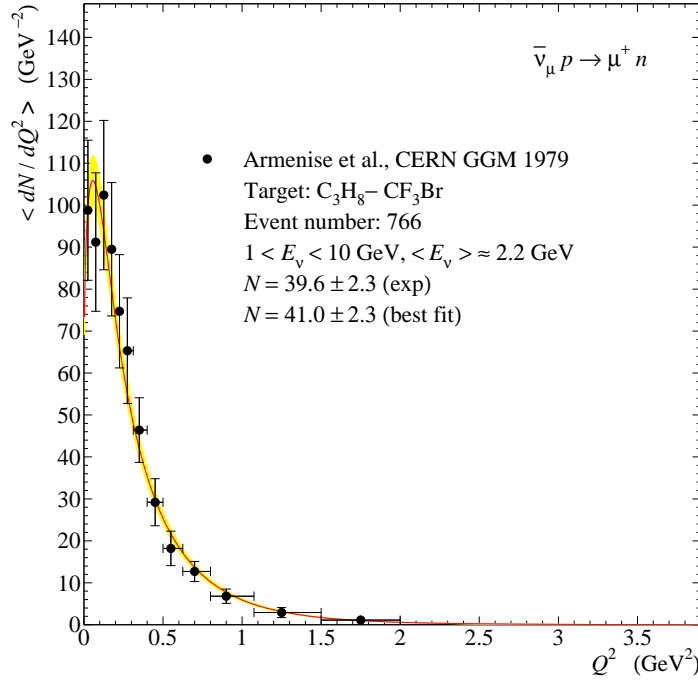


Fig. 16. Flux-weighted Q^2 distribution for $\bar{\nu}_\mu p \rightarrow \mu^+ n$ measured with the bubble chamber Gargamelle filled with light propane–freon mixture (87 mole per cent of propane) and exposed to the CERN-PS $\bar{\nu}_\mu$ beam [56]. The error bars contain both statistical and systematic errors. The curve is the distribution calculated with M_A obtained from the global fit, averaged over the experimental $\bar{\nu}_\mu$ energy spectrum from Ref. [56], and normalized to the GGM 1979 data. The energy range and estimated mean energy are given in the legends. Shaded band represents 1σ variation from the average due to uncertainties in M_A and normalization factor N .

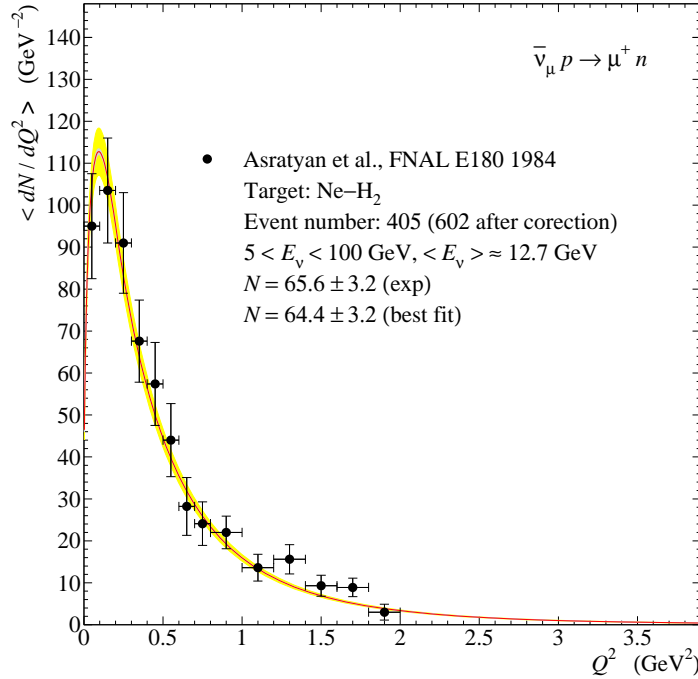


Fig. 17. Flux-weighted Q^2 distribution for $\bar{\nu}_\mu p \rightarrow \mu^+ n$ measured in the FNAL E180 experiment with a 15' bubble chamber filled with heavy neon–hydrogen mixture (64% of neon atoms) and exposed to the FNAL wide-band $\bar{\nu}_\mu$ beam [33,34] (see also Ref. [31] for an earlier version). The curve is the distribution calculated at the mean antineutrino energy of 12.7 ± 0.2 GeV, with M_A obtained from the global fit and then normalized to the E180 data. [The spectrum averaging procedure cannot be applied here, since the $\bar{\nu}_\mu$ spectrum has been evaluated just from the quoted Q^2 distribution.] Shaded band represents 1σ variation from the average due to uncertainties in M_A and normalization factor N .

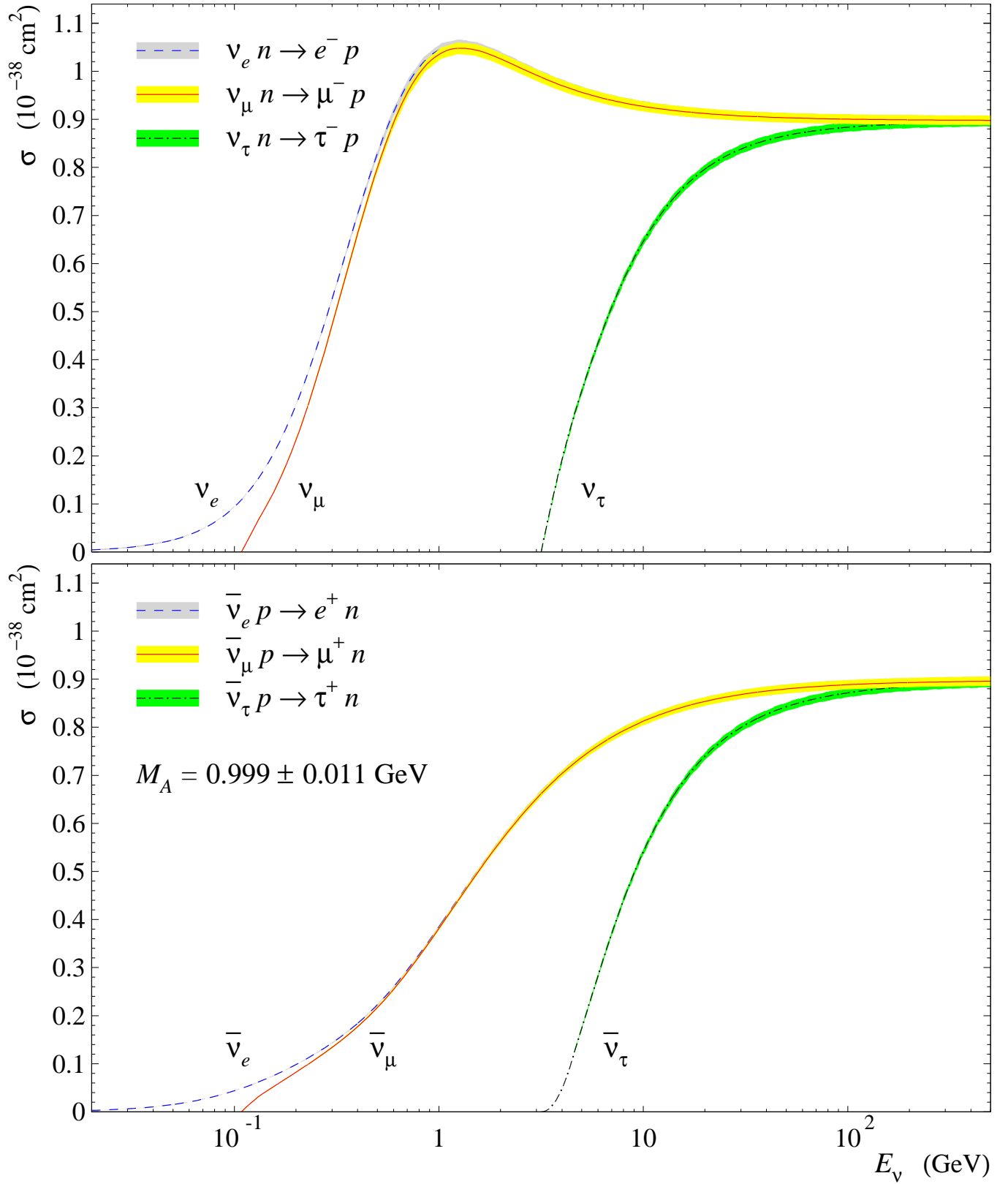


Fig. 18. Total quasielastic cross sections for electron, muon and τ neutrino and antineutrino interactions with free nucleons calculated with the best-fit value of $M_A = 0.999 \pm 0.011 \text{ GeV}$ using the BBBA(07) vector form factors. Shaded bands represent the uncertainty due to the 1σ error in M_A .

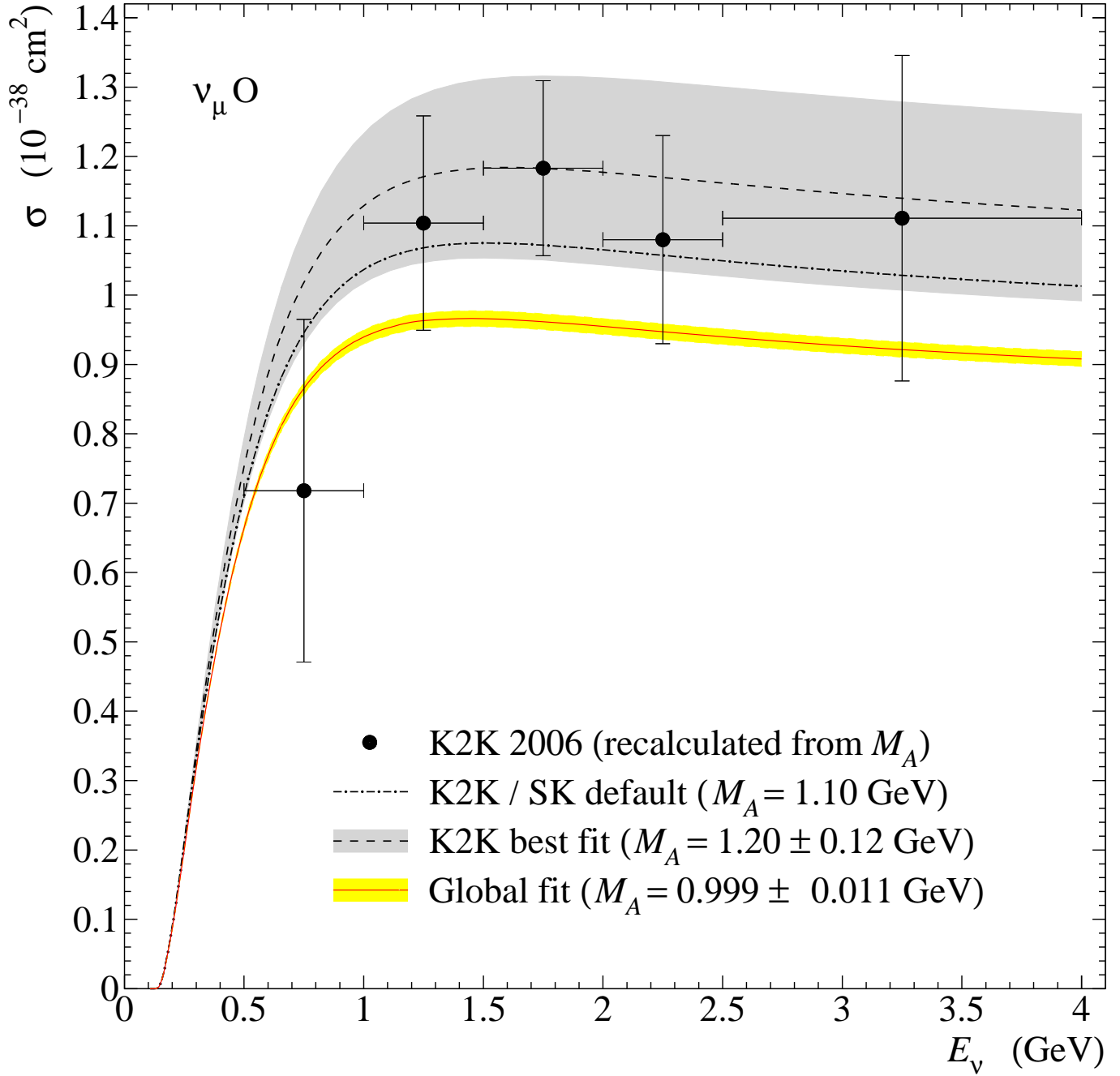


Fig. 19. Comparison between the QES ν_μ cross sections per neutron bound in oxygen, evaluated with several values of the axial mass. The solid curve with narrow band is calculated with our best fit value of M_A ; the dashed curve with wide band corresponds to the K2K extraction of M_A [4]; the dash-dotted curve is calculated with the current K2K and Super-Kamiokande I default $M_A = 1.1 \text{ GeV}$ [119,120]. The points represent the K2K cross section reconstructed (with our version of RFG model and BBBA(07) vector form factors) from the best-fit values of M_A extracted for the five energy bins, as quoted in Fig. 9 of Ref. [4].

